

Journal of Climate

The Influence of Volcanic Eruptions on the Climate of South America during the Last Millennium --Manuscript Draft--

Manuscript Number:	JCLI-D-14-00218
Full Title:	The Influence of Volcanic Eruptions on the Climate of South America during the Last Millennium
Article Type:	Article
Abstract:	<p>Currently, little is known on how volcanic eruptions impact large-scale climate phenomena such as paleo-ITCZ position or South American Summer Monsoon behavior. In this paper, an analysis of observations and model simulations is employed to assess the influence of large volcanic eruptions on the climate of South America. This problem is considered both for historically recent volcanic episodes, for which more comprehensive global observations exist, as well as reconstructed volcanic events for the period 850 C.E. to present that are incorporated into the NASA GISS ModelE2-R simulation of the Last Millennium. An advantage of this model is its ability to explicitly track water isotopologues throughout the hydrologic cycle, to predict the anticipated isotopic imprint following a large eruption, and to remove a degree of uncertainty when comparing the GISS simulations to paleoclimate proxy archives.</p> <p>Our analysis reveals that both precipitation and oxygen isotope variability respond with a distinct seasonal and spatial structure across South America following an eruption. During austral summer, there is enrichment in the heavy oxygen isotope in precipitation associated with reduced moisture convergence in the ITCZ and reduced rainfall over northern South America. In contrast, there is a relative depletion of the heavy oxygen isotope during the austral summer despite reductions in monsoon precipitation, suggesting that temperature is important for understanding the tropical South American isotopic response to large volcanic eruptions. Several of the robust responses directly affecting South America's hydrologic cycle are explored.</p>

Response to Reviewer 1

We thank Reviewer 1 for the time spent reviewing our manuscript, and are encouraged by the recommendation to accept. We have made several changes to the paper since the last review, hopefully for the better. We have fixed the references section and supplementary figures are included.

Response to Review #2

First, we thank Reviewer #2 (R2) for the time spent examining our paper.

R2's primary criticism emerges from the poor agreement that we showed (in the initial manuscript) between the modeled and observed climate response to the three largest eruptions (L20) since 1960. R2 further raises some methodological questions and seeks clarification on several aspects of the presentation of our material. Finally, R2 objects to the fact that some results in our study are "noisy," which calls for a more thorough justification on why our results ought to be published. In this response, we **(1)** defend and clarify the methods used in the study, and **(2)** re-frame the problem of historical comparisons between models and observations.

With respect to point **(2)**, a core issue is that the regional details of how temperature, precipitation, etc. vary in the historical record (or in individual model runs) are themselves noisy and not pure responses to external forcing. This is true even after the effects of ENSO are removed statistically. Since the regional response to volcanic eruptions, not just in South America but almost everywhere, is generally eruption-dependent (and ensemble member dependent) and tied to the background internal variability, and because observations themselves are just one realization of many possible realities, **we argue that a regional historical model-observation comparison over three eruptions should not form the backbone for hypothesis testing.** This is not a unique obstacle for ModelE2-R. Indeed, other results, such as those recently published in this journal (Fig. 1 and 2 in Man et al., 2014) with the MPI-ESM simulation reveal many regional mismatches in response between individual realizations (both with respect to each other and to observations), including over South America.

Although model error invariably contributes to such mismatches, even a perfect model would be of limited use for regional interpretations due to the signal-to-noise problem we are dealing with during the historical period. For this reason, and following the suggestion of another reviewer, we have removed the L20 temperature and precipitation spatial composites of the ensemble mean/observations that were presented in the previous manuscript. Instead, we show super-posed epoch analyses of tropical-mean temperature and precipitation anomalies after the recent two L20 eruptions (post-satellite era). Furthermore, in the paper we show two twelve panel plots (for temperature and precipitation) of the observed and six-member ensemble mean after each eruption. In the text, we highlight areas of agreement, disagreement, and in particular where disagreement can be understood without appealing to model error. Additionally, we highlight the climatological seasonal cycle of precipitation and oxygen isotopes in the model, which agrees well with observations.

Because the information that can be obtained from observations is limited, this is ultimately why we wish to move forward with a larger sample of last millennium

volcanic events that (in our composites) feature more events and of higher-amplitude. All of the results presented in this study are, in principle, falsifiable with an appropriate high-resolution network of proxies, and could also be compared to other isotope-enabled modeling results by other groups as a test of robustness.

Finally, it is important to emphasize that almost nothing is known about how the South American climate ought to respond to volcanic forcing or what paleoclimatologists ought to find (if a sufficiently well-resolved network of proxies, recording isotopic anomalies, were obtained). It is in this spirit that we believe our results are novel and useful.

In the following, a more detailed response to R2's criticisms are given (all figure numbers refer to those in this reply unless otherwise stated):

Minor Comments-

Incorrect reference, Robock et al to Robock, 2000: Fixed.

Statement on aerosols being injected into atmosphere: Clarified.

Oxygen to water isotopologues: Fixed.

ENSO definitions: Defined.

References in AMS format: Fixed.

Major Comments-

In the following, we illustrate the spread in observed responses for the L20 eruptions described previously. Figure 1 below compares observations of JJA temperature anomalies (using two seasons after the eruption subtracted from the previous five years after the effects of ENSO are removed) and the six-member ensemble mean from ModelE2-R for each L20 eruption. In the paper we show both seasons, and with a slightly different regression procedure (regressing out Niño 3.4 compared to the Niño 3 region). Figure 2 then shows six different realizations to the Mt. Pinatubo eruption only (the largest of the three eruptions) in the model, each of which is forced identically but is occurring against different background initial conditions in the simulation.

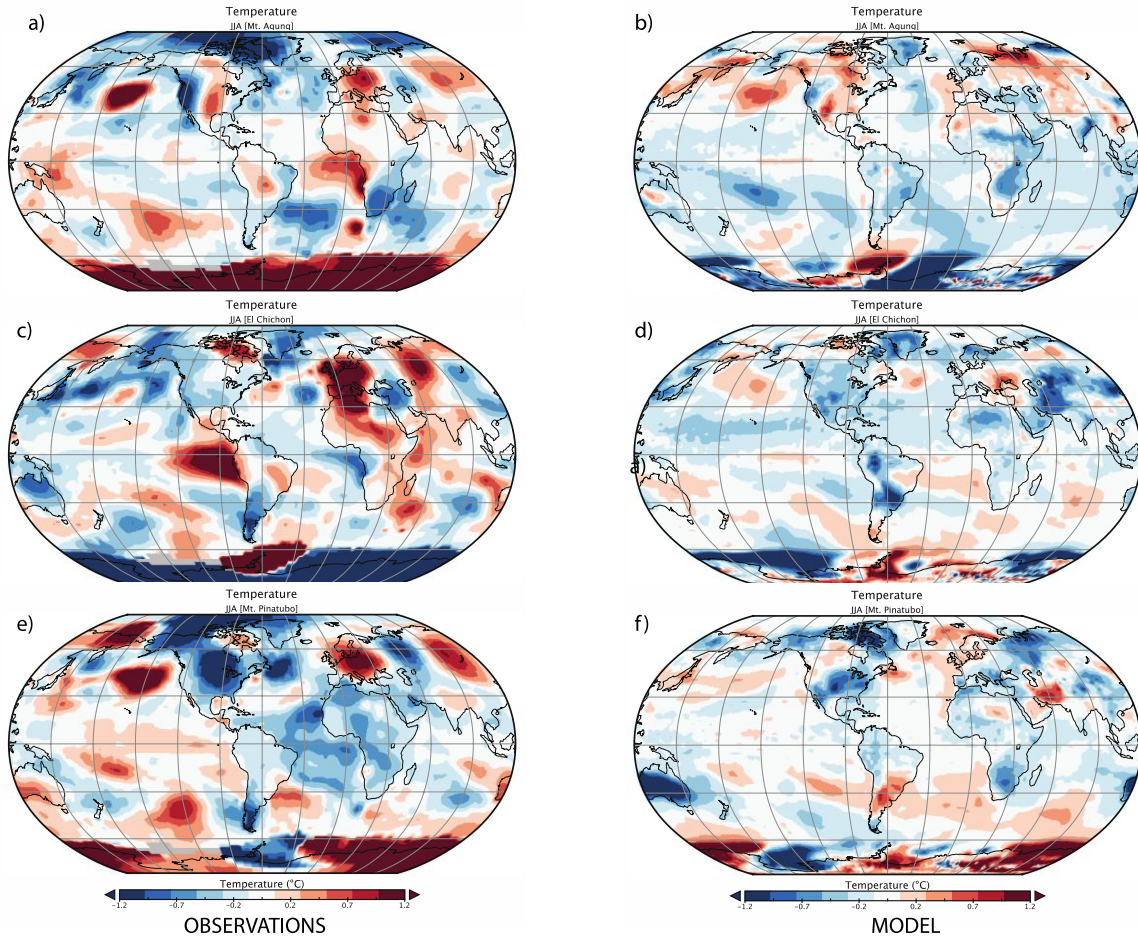


Figure 1) Temperature anomaly in JJA (two seasons after each eruption relative to previous five years) for (a)(b) Mt. Agung, (c)(d) El Chichón and (e)(f) Mt. Pinatubo. The left-hand column is the observations using the GISTEMP land+ocean temperature index and the right column is from GISS ModelE2-R.

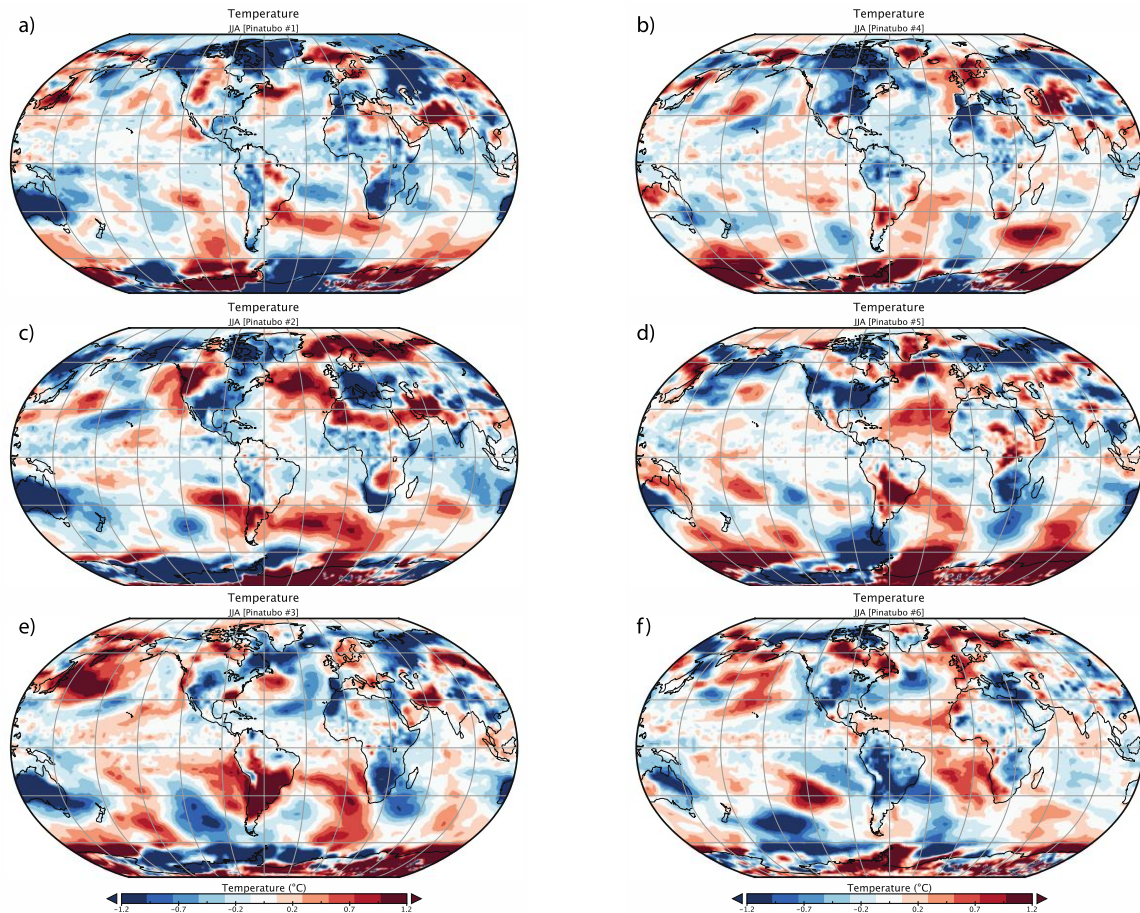


Figure 2) Temperature anomaly in JJA for Mt. Pinatubo in six different realizations to the same forcing with GISS ModelE2-R.

As is shown, there is a rather robust cooling (on a global scale) after these historical eruptions but with considerable spatial structure in the response. Similar variability is seen in temperature for DJF and for precipitation (see new manuscript). Over South America, much of the continent exhibits cooling immediately following most events, although some ensemble members (e.g., panel *e* in Figure 2) exhibit widespread warming south of the equator. Figure 1 shows that there is still an ENSO imprint on the observed temperature response after El Chichón that is not reproduced by the model; the influence of El Niño is much stronger (especially for El Chichón and Mt. Pinatubo) if it had not been regressed out beforehand. Nonetheless, a residual warming in northern South America remains that is not associated with external forcing and should not be expected to be a prominent feature in model composites.

In the text for the revised manuscript, we justify the use of ModelE2-R on the basis that it is skillful in simulating climatological rainfall, including the seasonal cycle of precipitation and oxygen isotopes, over South America. We also include Figures 3 and 4, each a super-posed epoch analysis of the tropical temperature and

precipitation response to the recent L20 eruptions (excluding Mt. Agung). Descriptions of these figures are in the caption.

The GISS ModelE2-R captures the magnitude and duration of tropical (25°S-25°N, all longitudes) cooling following the two recent L20 eruptions. For precipitation, there is a reduction in model rainfall although the observations exhibit a less clear signal. Although there is a reduction in rainfall during the first year of the eruption composite (now excluding Mt. Agung), the observations show a recovery faster than the model. This recovery is largely due to the later part of the El Chichón eruption. The observed rainfall decrease is more pronounced if Mt. Pinatubo is considered in isolation (not shown).

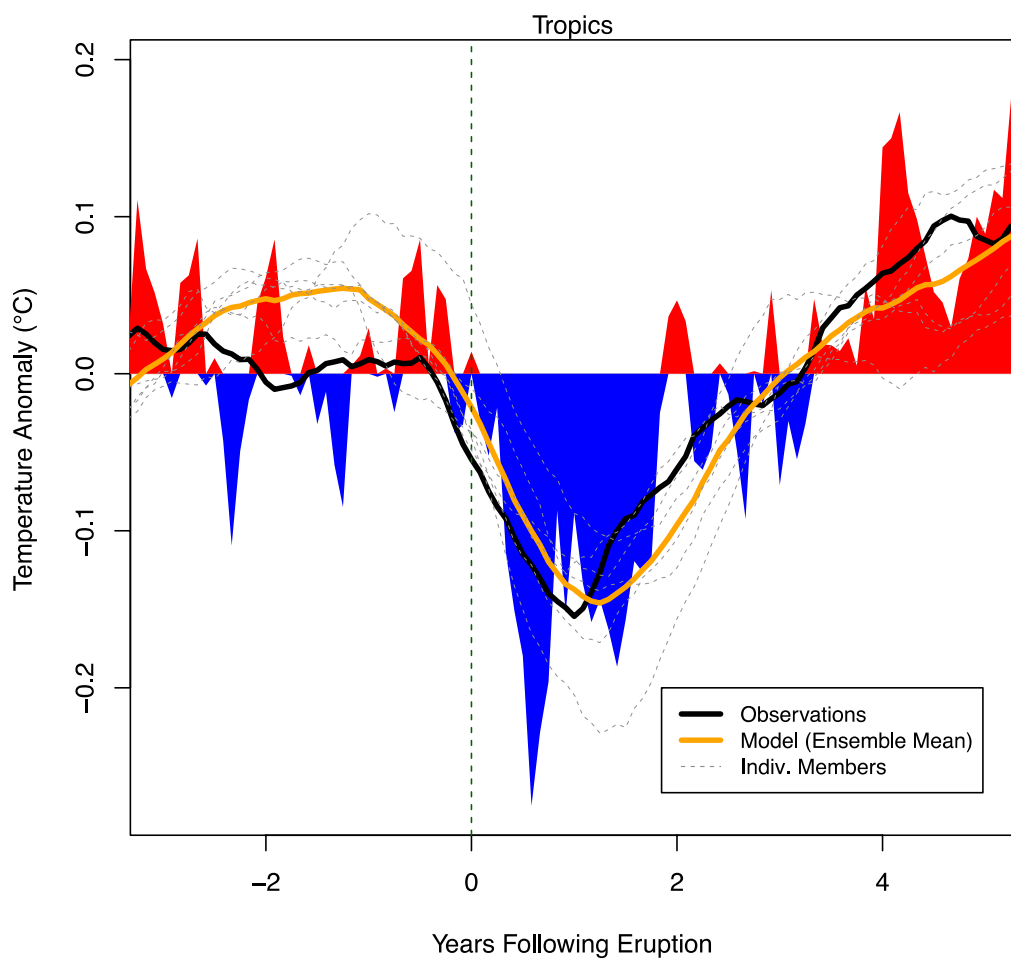


Figure 3) Super-posed epoch analysis of monthly tropical-mean temperature anomalies associated with El Chichón and Mt. Pinatubo (ENSO removed and composited) from year -3 to 5 (eruption month corresponding to zero). Monthly-observed anomalies from the GISTEMP land+ocean temperature index shown in fill color. The black solid line is the 18-month running mean of these temperature anomalies. Additionally, the 18-month running mean of each ensemble member (grey dashed) and ensemble mean (yellow solid) is shown. All values are offset such that the mean value during the 8-year period shown is zero.

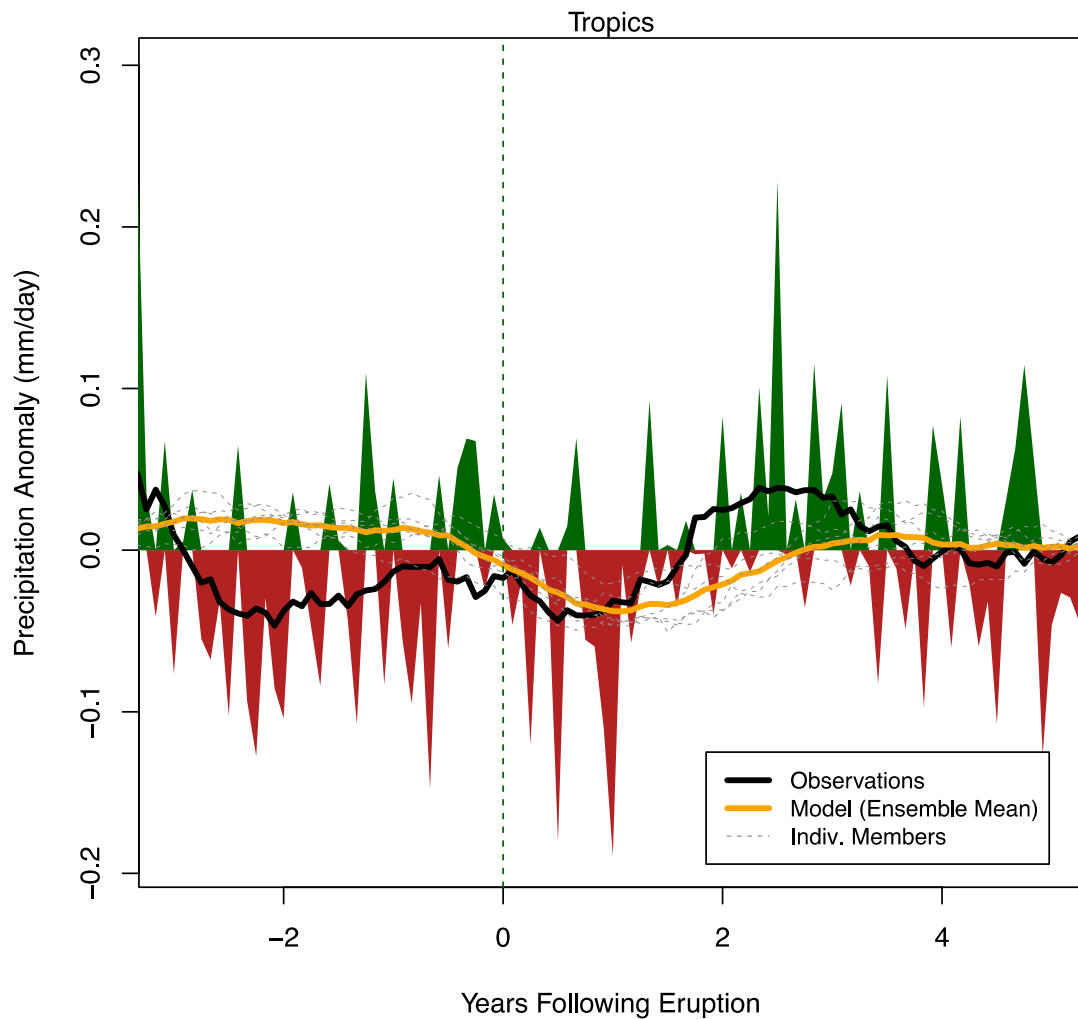


Figure 4) As in Figure 3 except for precipitation. Observations derive from GPCP v2.1.

These figures are reproduced in the revised manuscript with a more detailed discussion and references given. A further evaluation of the three historical eruptions is beyond the scope of this work. Nonetheless, we stress with these figures the skill in model performance and the variability expected to individual events.

Further Comments (reviewer comments in red)-

>What does this mean? The monsoon includes the entire year, with different phases.

This is actually not quite correct. The South American Summer Monsoon (SASM) is somewhat different from the global monsoon in the sense that there is no seasonal wind reversal as is observed, for example, over Asia (Zhou and Lau, 1998). Therefore the South American Monsoon is exclusively a summer season phenomenon, with an onset phase (Oct-Nov.), a mature phase (Dec.-Feb.) and a demise period (April-May). The rest of the year the SASM is absent. There is no such thing as a South American Winter Monsoon. There are detailed descriptions of the SASM and its phase locking to the austral summer in Vuille and Werner (Clim. Dyn., 2005); Vera et al. (BAMS, 2006); Garreaud et al., (Palaeo3, 2009); Marengo et al. (Int. J. Climatol., 2012) and Vuille et al. (Clim. Past, 2012).

>On the use of “fully-coupled” as a model description

>What does this mean, if ozone and aerosols appear to be specified, and not able to interact with the circulation?

The phrase “fully-coupled ocean-atmosphere model” is inserted for clarification. We did not mean to imply that every aspect of the Earth system is simulated, but that the model features a dynamic ocean (not a slab) and sea-ice that are all interacting.

>It is not clear how many climate model simulations are shown. How many ensemble members were carried out for how many years? It appears that there were only three model runs for different combinations of solar and land forcing. But there were no multiple ensembles for the same forcing but different initial conditions. Thus we are not able to examine the effects of chaos on the results.

We have clarified the text to emphasize that we used three simulations that were each run from 850-2005 C.E. In each of these three simulations, there are 16 volcanic eruptions that meet the AOD threshold criteria employed in this study; thus there are $16 \times 3 = 48$ events that are averaged for the generation of all LM composites.

Since the composite response is composed of just two seasons after each eruption (relative to the surrounding climatology), the effects of solar/land-use differences among the ensemble members are negligible in this context. This would not be true if these other forcings exhibited much higher-amplitude and higher-frequency variability that was coincidentally timed with several of the eruptions used in the composite, but this is not the case. Thus, the differences among the simulations can be attributed exclusively to differences in the model background internal variability at the time of the eruption. In this sense we are working with an ensemble.

To verify this expectation, we looked at temperature and precipitation using ModelE2-R simulations that differed in solar/land-use forcing but featured no volcanic forcing. We created a composite map averaging over the same dates during the Last Millennium as were used in the volcanic composites presented in the study.

Not only is there a lack of any notable response in South America that is present in the volcanic composites, but also there is no indication of any forced differences among the ensemble members.

Unfortunately, running fully coupled >1000 year simulations is very costly and we are constrained to utilizing only a few simulations, as is commonly the case with studies relying on complex GCMs. However, we note that volcanic forcing is very large and thus averaging over $16n$ (where n is the ensemble size) number of events would be expected to yield a coherent signal even for a small n , especially since we are restricting our results to large eruptions. Below, we present evidence of this.

The following four multi-panel plots (Figs. 5-8) show results for composite temperature and precipitation (both seasons) using various combinations of the three ensemble members that use the Crowley forcing, as discussed in the paper. In each plot, the season is identified along with the particular combination of ensembles averaged over (ck= Pongratz/Krivova; ckk=Kaplan/Krivova; cs=Pongratz/Steinilber to denote the land-use/solar forcing, respectively). In each plot, the top panel displays averages over all three members for a total of 48 volcanic events, the left column displays results for each single simulation (each an average of its own realization of the 16 eruptions), and the right column shows the average of different combinations of two ensemble members.

For each variable and season, even averaging over just 16 events ($n=1$, as in the left column of each panel produces nearly the same pattern of anomalies as for 32 or 48 events. This breaks down somewhat over the wintertime mid-latitudes as might be expected, but the differences among the ensemble members are notably less across the tropics. Thus, there is evidence that averaging over just 16 realizations is sufficient to extract the signals of interest in this study, if such a signal exists. There is no reason to expect that moving to $n=4,5,6$, etc. will suddenly reveal anything further of interest for our purposes.

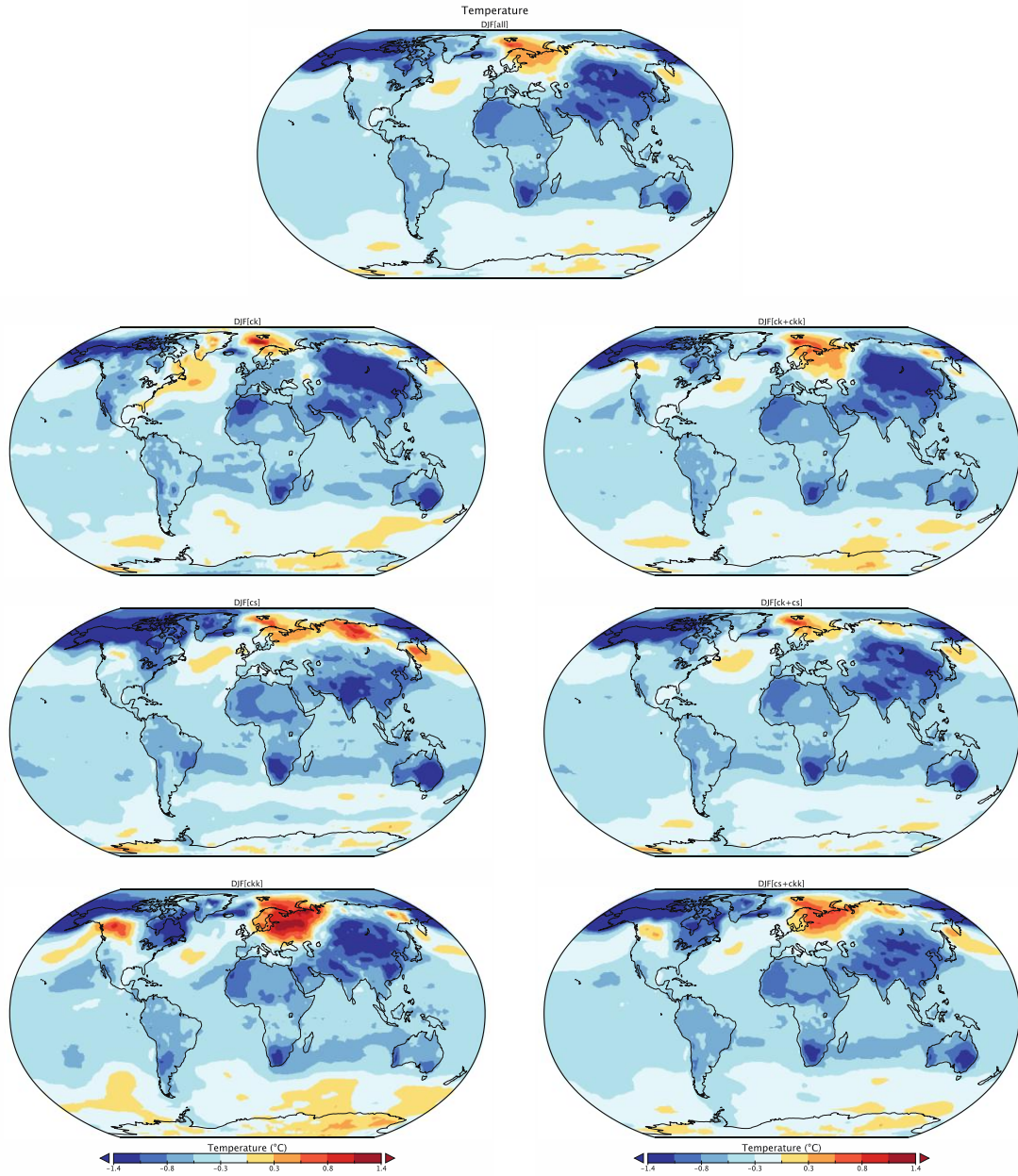


Figure 5) Composite temperature response (DJF) to a volcanic forcing using different combinations of ensemble runs.

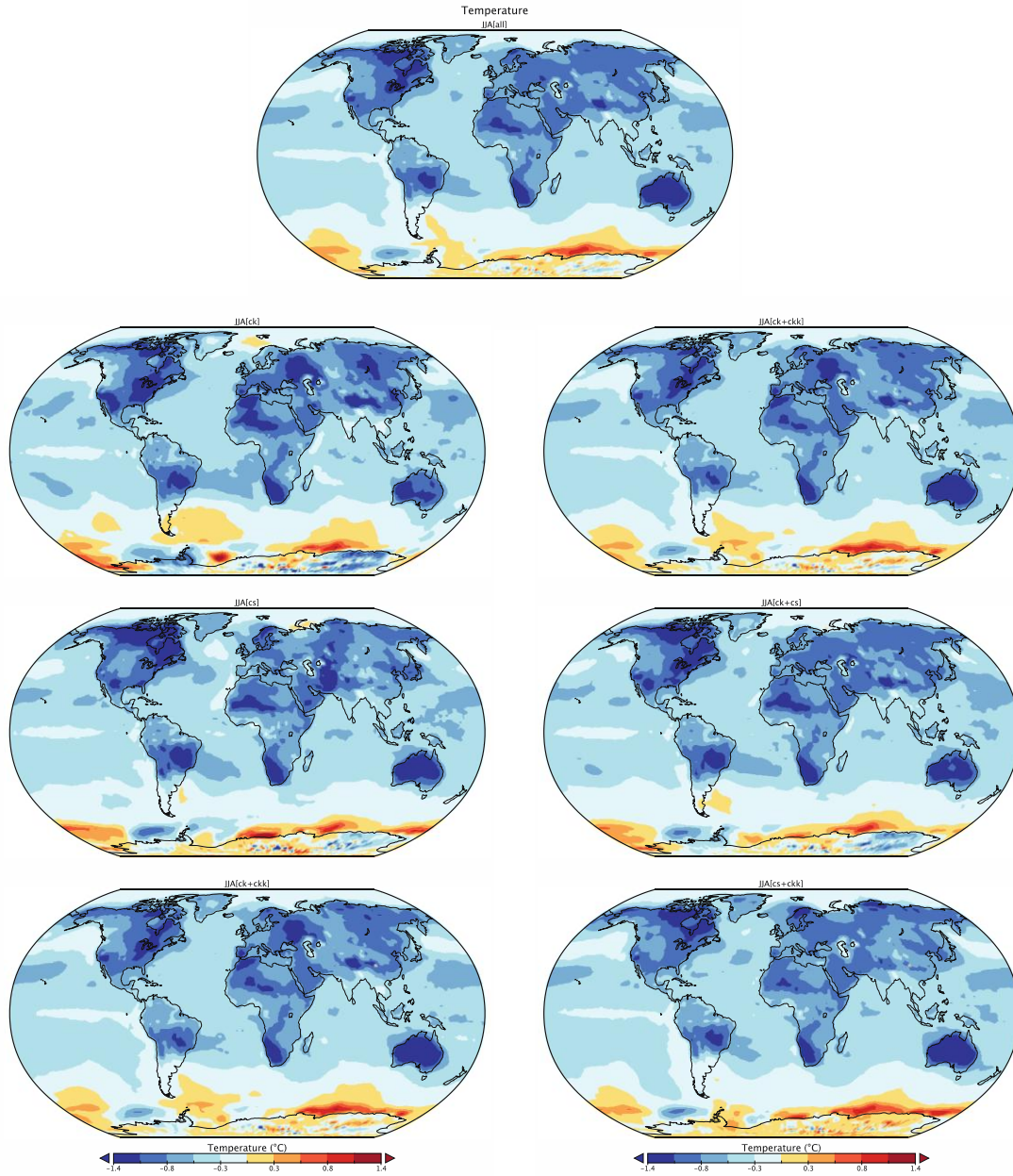


Figure 6) Composite temperature response (JJA) to a volcanic forcing using different combinations of ensemble runs.

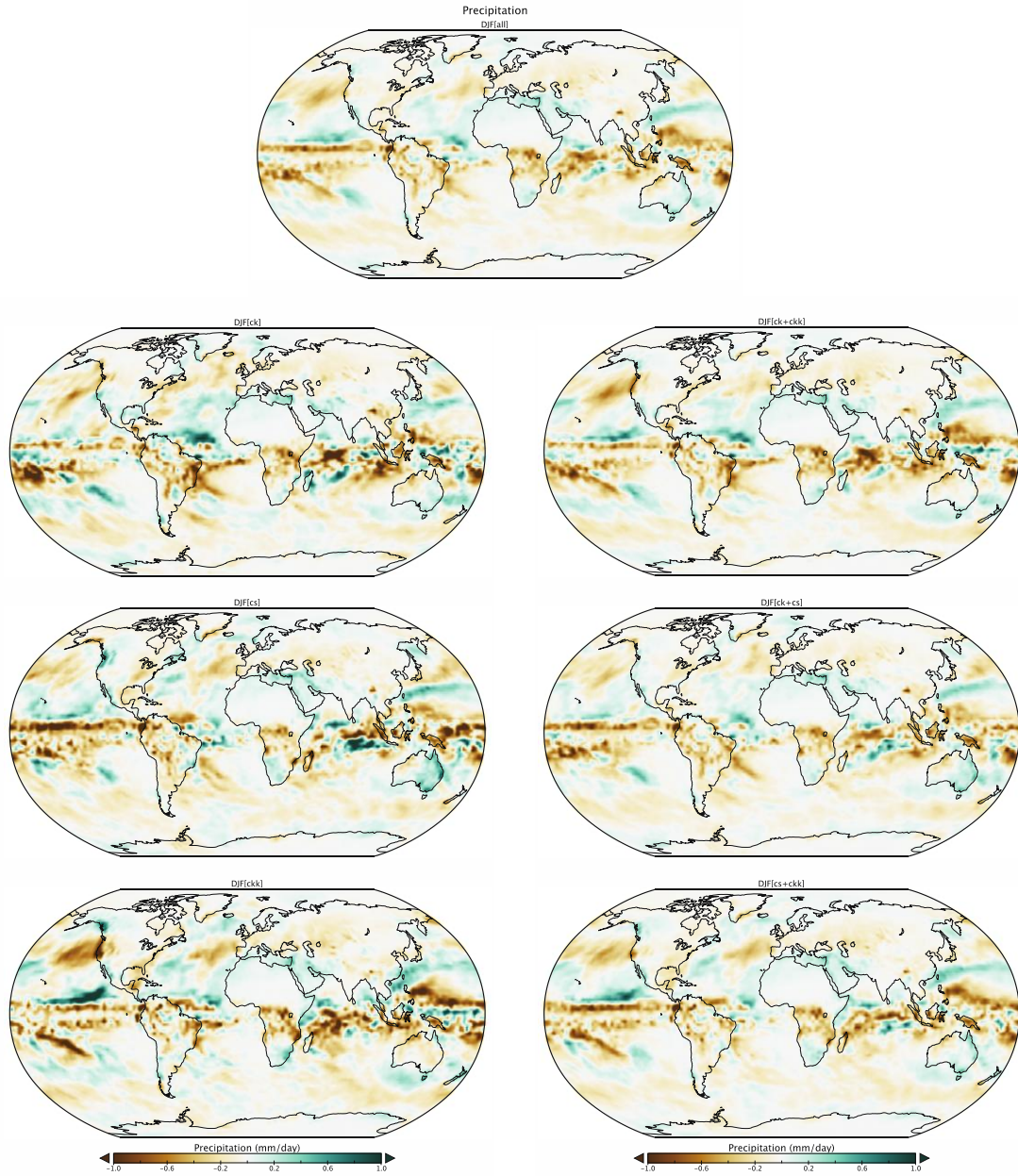


Figure 7) Composite precipitation response (DJF) to a volcanic forcing using different combinations of ensemble runs.

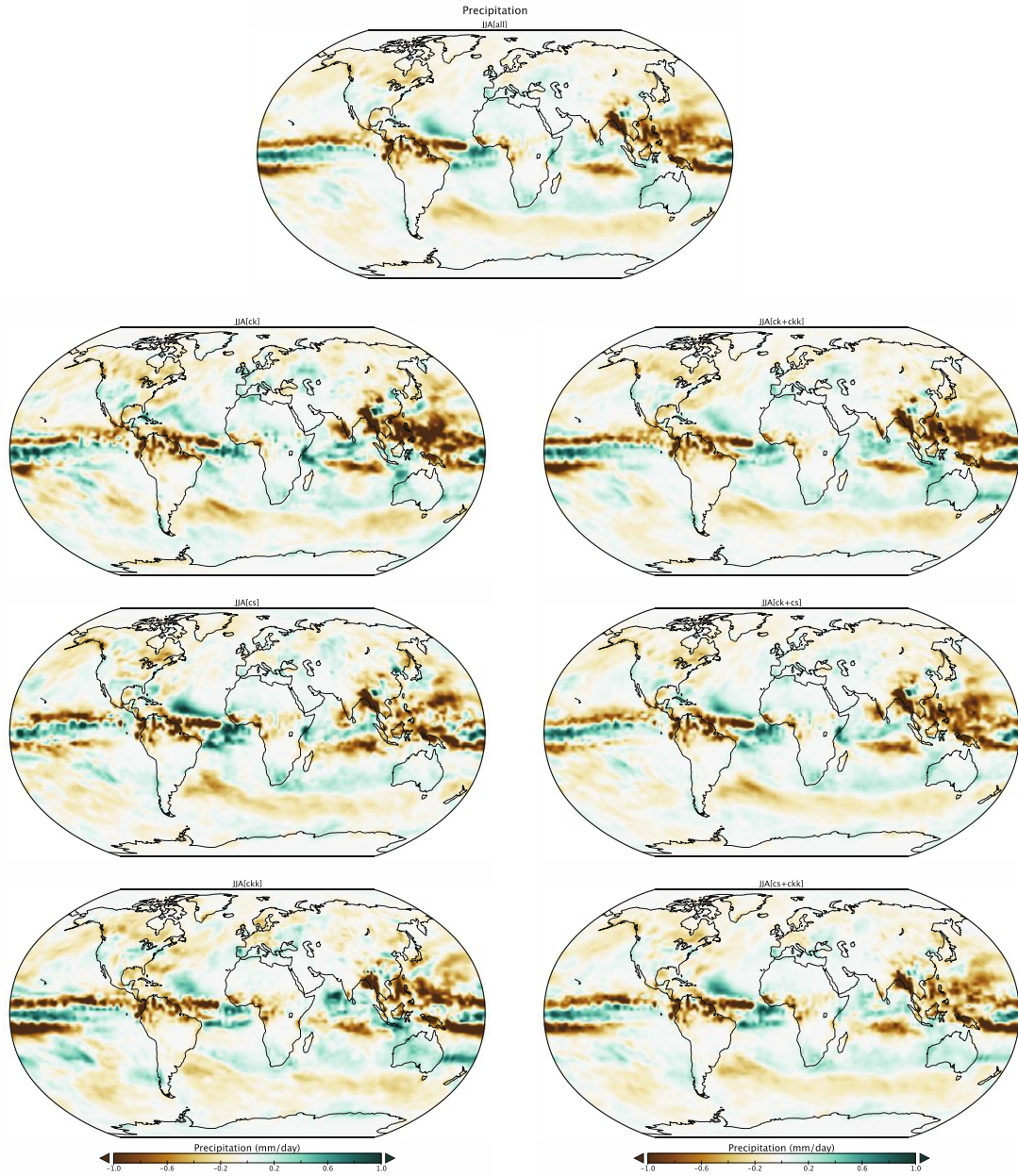


Figure 8) Composite temperature response (JJA) to a volcanic forcing using different combinations of ensemble runs.

>But it appears that Fig. 2 is for the climate surrounding volcanic eruptions. What is >the non-volcanic climate? Show that, and then anomalies.

In the paper, we show Figure 2 to illustrate the model representation of the seasonal cycle (expressed as a ratio of seasonal to annual precipitation). The reviewer is concerned with the fact that we show the climate surrounding volcanic eruptions rather than the “non-volcanic climate.” This was intentional, since we did not want to compare the volcanic anomaly to a climatology that was far removed from the time of eruption, in order to include the possibility of low-frequency trends in the simulation that are not of interest in our composites (note there is no actual non-volcanic climate in the simulations forced with volcanoes).

The composite in Figure 2 of the revised manuscript represents an average of slightly less than $15 \times 2 \times 16 \times 3 = 1440$ seasons (i.e., 15 seasons on each side of each eruption, times 16 eruptions, times three ensemble members). In reality we average 1269 values per grid cell due to a few seasons where two eruptions overlap, and because the last two eruptions use only five years prior to the eruption. The composite does not include the volcanic seasons themselves.

These are more than enough seasons to sample the seasonal cycle. To show that the choice of climatology is irrelevant for the construction of Figure 2, we show here (Fig. 9) the average of all DJFs and JJAs in the Figure 2 composite (as described above) vs. the average of all DJFs and JJAs in the entire Last Millennium simulation. There is virtually no difference between these composites (this is not plotted incorrectly, a difference map would reveal that the columns on the left and right differ usually by decimal places). This is also true over the ocean. Thus, the use of 1269 seasons to create an average illustrating the model’s climatology is fully justified.

Climatological Precipitation (Last Millennium)

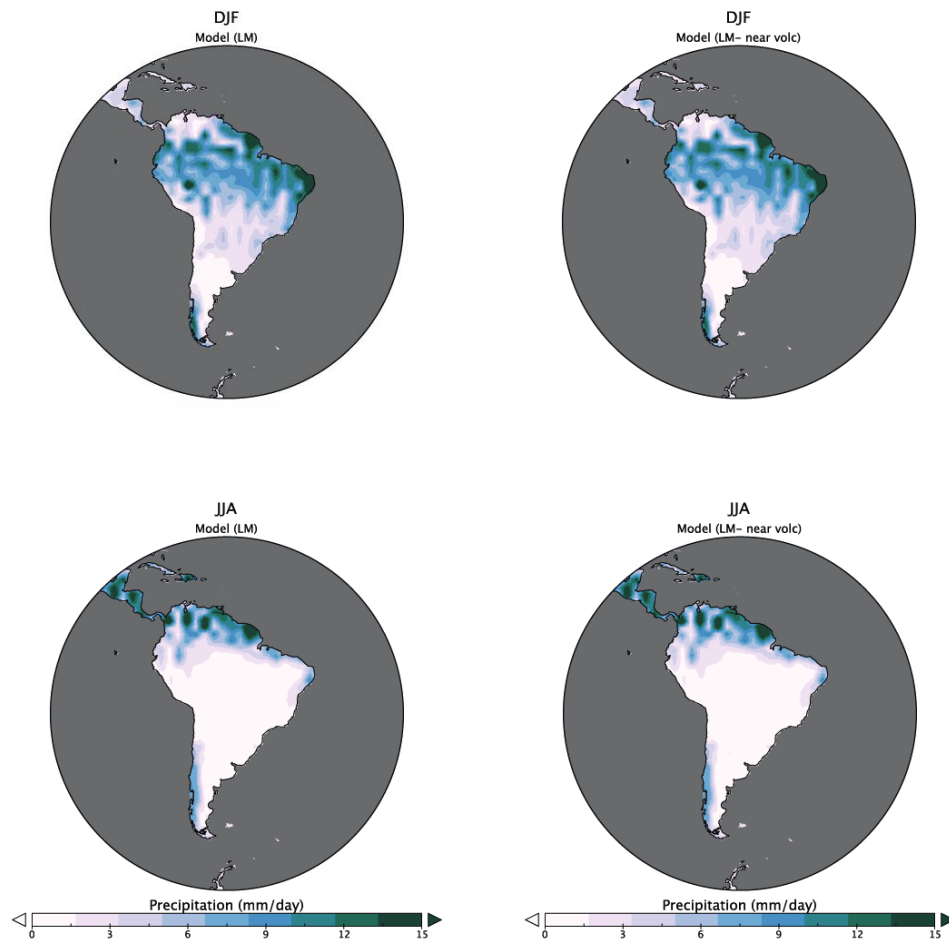


Figure 9) Land precipitation in the LM composite using the method described in text (15 seasons surrounding each eruption, right column) and using all seasons in the simulations (averaged over three ensemble members, left column).

*>The results are eruption-dependent and overwhelmed by natural variability
>in the model simulations. Does this mean that we cannot expect any
>coherent precipitation response to the next large volcanic eruption?
>Certainly many ensemble members could have given us some quantitative
>assessment of this.*

There are many clear responses that we presented in this study, and the point about ensemble size has been addressed previously. We were indeed surprised by the lack of sizable response in precipitation over much of South America during the austral

summer, and we did in fact highlight the eruption-dependency in the Supplementary figures and text.

If the common “signal” is indeed that there is only a weak coherent signal (as was reported for DJF precipitation in the core monsoon region of South America) then we find this interesting and important too. For this reason, we showed results for individual eruptions in the Supplementary info (Figure S4). The result is not that there is no response (indeed, there is a reduction in precipitation over parts of the continent in the composite, and also see the new histogram (Figure 12 in the updated manuscript that shows the average rainfall anomaly in the core monsoon region to be an outlier among 100-random 48-event composites in a control simulation). Nonetheless, it is not self-evident that rainfall during the monsoon season should care only weakly about volcanic forcing vs. internal variability. In summary, we disagree that this stands as a “negative result.” It is also not uninteresting that the structure or sign of climate signals/trends are highly dependent on the state of internal variability in the presence of external forcing (see e.g., Deser et al., 2014).

However, clear results do emerge during JJA in regions that, climatologically, still experience strong rainfall (north of the equator) and also in the temperature/oxygen isotope expression over much of South America (including DJF). For these last millennium composites, all results are masked for statistical significance; furthermore, the superposed epoch figure (presented as a Hovmöller) highlights notable anomalies in several critical climate variables that are presently not discussed in a South American context in the current literature.

>The authors only show DJF and JJA results, thus leaving out half of all >the data. Why are not all the seasons shown?

This choice is fairly standard practice in South American climate literature, since DJF and JJA represent the two well-defined wet (monsoon) and dry seasons, respectively, over much of the continent. MAM and SON represent transition seasons that partially cover dry seasons and partially monsoon onset and demise over tropical and subtropical South America. Except for studies that explicitly target monsoon onset and demise or changes in length of monsoon duration, these seasons are usually omitted. Moreover, the paper is already long and we did not feel that increasing the number of seasonal composite results by a factor of two would be sensible.

However, the Hovmöller diagram in Figure 11 of the revised paper is computed based on monthly anomalies, and so the evolution of temperature, precipitation, and oxygen isotopes during the transition seasons can be inferred.

Finally, we note that most figures have been improved since the previous manuscript. The last Hovmöller diagram did indeed feature a color scale, despite the

reviewer suggesting otherwise, although this figure was improved as well for color-bar consistency.

References:

- Deser, C., A. S. Phillips, M. A. Alexander, and B. V. Smoliak, 2014: Projecting North American Climate over the next 50 years: Uncertainty due to internal variability. *J. Climate*, **27**, 2271-2296.
- Garreaud, R. D., Vuille, M., Compagnucci, R., and Marengo, J., 2009: Present-day South American climate, *Palaeogeogr. Palaeoclimatol., Palaeoecol.*, **281**, 180–195.
- Huffman, G. J., R. F. Adler, D. T. Bolvin, and G. Gu, 2009: Improving the global precipitation record: GPCP Version 2.1, *Geophys. Res. Lett.*, **36**, L17808.
- Marengo, J. A., Liebmann, B., Grimm, A. M., Misra, V., Silva Dias, P. L., Cavalcanti, I. F. A., Carvalho, L. M. V., Berbery, E. H., Ambrizzi, T., Vera, C. S., Saulo, A. C., Nogues-Paegle, J., Zipser, E., Seth, A., and Alves, L. M., 2012: Recent developments on the South American monsoon system, *Int. J. Climatol.*, **32**, 1–21.
- Man W., T. Zhou., and J.H. Jungclaus., 2014: Effects of Large Volcanic Eruptions on Global Summer Climate and East Asian Monsoon Changes during the Last Millennium: Analysis of MPI-ESM Simulations. *J. Climate*, **27**, 7394–7409.
- Vera, C., Baez, J., Douglas, M., Emmanuel, C. B., Marengo, J., Meitin, J., Nicolini, M., Nogues-Paegle, J., Paegle, J., Penalba, O., Salio, P., Saulo, C., Silva Dias, M. A., Silva Dias, P., and Zipser, E., 2006: The South American low-level jet experiment, *B. Am. Meteorol. Soc.*, **87**, 63–77.
- Vuille, M. and Werner, M., 2005: Stable isotopes in precipitation recording South American summer monsoon and ENSO variability – observations and model results, *Clim. Dynam.*, **25**, 401–413.
- Vuille, M., S.J. Burns, B.L. Taylor, F.W. Cruz, B.W. Bird, M.B. Abbott, L.C. Kanner, H. Cheng and V.F. Novello, 2012: A review of the South American monsoon history as recorded in stable isotopic proxies over the past two millennia. *Clim. Past*, **8**, 1309-1321.
- Zhou, J., and K.-M. Lau, 1998: Does a monsoon climate exist over South America? *J. Climate*, **11**, 1020-1040.

Response to Review #4

First, we thank Reviewer #4 (R4) for the time spent on examining our paper. The quality of the new manuscript has improved considerably due to a consideration of several issues raised by R4.

Here, we reply to several of R4 points (reviewer comments in red). There is some redundancy in the R4 response, so we cover the salient points:

>> 2. Introduction: restructure to introduce the reader to (0) motivating question: tropical/subtropical hydroclimatic response to volcanic external radiative forcing; (1) estimating the forcing itself (from indirect observations of various sorts), in location, time, amplitude, nature of the aerosols; (2) estimating the response to the forcing, via climate and isotope forward modeling; (3) observations of the tropical hydroclimatic response, given their uncertainties (location, time, amplitude), with emphasis on South American mechanisms of hydroclimatic response.

>>In general I think the introduction could be better structured, to introduce the reader to the various elements going into volcanic forcing experiments: (1) estimating the forcing itself (from indirect observations of various sorts), in space, time, amplitude, nature of the aerosols; (2) estimating the response to the forcing via climate modeling; (3) assessing the degree to which there is agreement with observations of the climatic response, give their uncertainties (space, time, amplitude); (4) focus on the problem particularly for South America. These are global models, why focus on a small part of the globe? Especially as there may be multiple response mechanisms (e.g. via SAMS/ENSO, SACZ, ITCZ) for which it may be difficult to make precisely attribution [but draw on Vuille et al 2012 more explicitly, which calls them independent in this paper - l. 203-204. The focus of this paper on South America should be better justified beyond the rationale at l. 179-186 - expand what is in the last part of the last sentence of this paragraph. It might be valuable, for both modeling, interpretation of results, and comparison with observations, to show the full global tropics (or global tropics + southern Hemisphere), and then focus interpretation with respect to South America.

>> 6. The introduction should propose a working hypothesis for the study: what do you expect to see in the modeling? How will you test it? I don't see these basic elements of experimental design, but they are implicit in the results. State and support them up front.

The introduction in our paper has been revised since the last version. We still retain sections relating to South American climate (both in terms of dynamics relevant for

the modern climate, and also a brief overview of paleoclimate issues in this area of the world), the influence of volcanic eruptions in general, and move toward a discussion of the model itself in the methods. This paper covers a lot of ground that cuts across the interface of modeling, observations, paleoclimate, and climate dynamics at a continental to tropical scale, and so we believe it is important to briefly address each of these aspects in the introduction. We have clarified the motivation for this study and hopefully answered all of the points above. Additionally, we have justified our focus on South America specifically.

4.1. Composite results shown in Figs 8 and 12, except for the global
>> tropics, since what happens over the global tropics is important for
>> the response over South America.

We address the tropical response in section 3.2b of the revised manuscript.

7. Since the L20 period contains only a few composite members,
>> consider making a complete 850-2000 composite, with more members, and
>> de-emphasizing the comparison with modern observations, because, as
>> you show, it is quite limited. Are there other isotope-enabled, 20th
>> c. simulations, that could be accessed for this exercise, b/c there
>> might be more reliability of interpretation in a multimodel ensemble?

>> 9. Fig 3: it looks like there is no relationship between the forcing
>> and the responses.

>>

>> 10. l. 461-462: Figs 3c,d, this is a weak statement on these results;
>> please show statistical testing to support the interpretation of the
>> results.

>>

>> 11. Figs 4, 5: mask for significance of anomalies, perhaps using
>> random draws of the same number of non-volcanic event years from the
>> L20 interval. How well supported are (what is the uncertainty in) the
>> observational maps given the sparsity of the data discussed in section
>> 1? Similarly, what is the mean difference between the ensemble
>> members? We should be convinced that the pattern of anomalies is
>> interpretable above the uncertainties in each case.

In the new paper, we have elected to move in a new direction with respect to the historical (L20) eruptions (see e.g., methods and section 3.1 of the revised manuscript). A recurring issue is the non-trivial nature of testing the T, P, or oxygen isotope fields robustly against the observations, at least on this very regional level. A more thorough investigation of the L20 mechanisms was never intended to be the primary goal of this study, but Figures 4-6 in the new paper are included in order to provide some guidance in interpreting the variability observed among the L20

events and the similarities/differences expected for an observation-model comparison during this time. There is a more extensive discussion in the revised manuscript along these lines. Ultimately, we want to focus on the Last Millennium composites, which capture a more robust signal.

>> 3.3. The composite response [agrees, disagrees] with global
>> tropical/SH hydroclimatic observations from proxy data; and here are
>> places where additional observations from proxy data would help
>> constrain interpretability of the simulations.

This is certainly an avenue for future research, but examination of proxy data is beyond the scope of this work. This is primarily a modeling study with a “new” model and unique rationale (exploring the isotopic response to eruptions). In essence, we hope to challenge the paleoclimate community to test the hypothesis put forth here.

> On statistical significance.

A critical point raised by R4 on several occasions concerns the statistical significance test (using a two-sided Student t-test) in which R4 argues that there are only 16 degrees of freedom available in the composites, and that significance should be recalculated accordingly.

Results: Revise all figures and results to mask for statistical
>> significance, keeping in mind (as done in Fig 9) that for degrees of
>> freedom estimates, that for the LM experiment there are 16
>> realizations of volcanic events, not 48. I suggest the paper would be
>> stronger and clearer if focused primarily on:

>> Did the statistical analysis rely on 16 realizations or 48? it should
>> be based on N=16 realizations. Each realization is based on three
>> estimates (ensemble members), just like an isotopic data value might
>> be based on triplicate measurements, but there are still only 16
>> volcanic eruptions to composite (as done in Fig 9, but here there
>> might be error bars on the ensemble averages).

>>8. l. 403-406: in the composite analysis, there are still only 16
>> degrees of freedom in making composites.

First, all last millennium composite figures have been reconstructed and masked for statistical significance. We state the statistical procedure we applied in the text. Moreover, the histogram (Figure 12) offers an additional perspective on the robustness of the LM results as a volcanic response.

However, we disagree with R4’s comments about the number of degrees of freedom. It is important to realize that each of the 48 events is an independent realization of the response to that forcing in ModelE2-R. Hence 48 is the correct n value. The

example offered by R4 of triplicate isotopic measurements is by no means an appropriate analogy in this respect, as in that case the same sample is tested three times to assess measurement uncertainty. In our case, we are dealing with uncertainty related to internal model variability, which has a different structure across all ensemble members at the time of the eruption.

Abstract

16
17
18
19
20
21
22
23
24
25
26
27
28
29
30
31
32
33
34
35
36
37
38

Currently, little is known on how volcanic eruptions impact large-scale climate phenomena such as paleo-ITCZ position or South American Summer Monsoon behavior. In this paper, an analysis of observations and model simulations is employed to assess the influence of large volcanic eruptions on the climate of South America. This problem is considered both for historically recent volcanic episodes, for which more comprehensive global observations exist, as well as reconstructed volcanic events for the period 850 C.E. to present that are incorporated into the NASA GISS ModelE2-R simulation of the Last Millennium. An advantage of this model is its ability to explicitly track water isotopologues throughout the hydrologic cycle, to predict the anticipated isotopic imprint following a large eruption, and to remove a degree of uncertainty when comparing the GISS simulations to paleoclimate proxy archives.

Our analysis reveals that both precipitation and oxygen isotope variability respond with a distinct seasonal and spatial structure across South America following an eruption. During austral summer, there is enrichment in the heavy oxygen isotope in precipitation associated with reduced moisture convergence in the ITCZ and reduced rainfall over northern South America. In contrast, there is a relative depletion of the heavy oxygen isotope during the austral summer despite reductions in monsoon precipitation, suggesting that temperature is important for understanding the tropical South American isotopic response to large volcanic eruptions. Several of the robust responses directly affecting South America’s hydrologic cycle are explored.

39

40 **1. Introduction**

41

42 1.1. Volcanic Forcing on Climate

43

44 Plinian (large, explosive) volcanic eruptions are a dominant driver of natural
45 climate variability during the Last Millennium (LM, taken here to be 850 C.E. – present),
46 including the last 50 years (Stothers and Rampino, 1983; Hansen et al., 1992; Crowley et
47 al., 2000; Robock et al., 2000; Robock, 2003; Goosse et al., 2005; Yoshimori et al., 2005;
48 Emile-Geay et al., 2008; Cole-Dai, 2010; Timmreck, 2012; Iles et al., 2013; Schurer et
49 al., 2014). As such, these eruptions serve as a natural testbed to assess the skill of climate
50 models in simulating how climate responds to external perturbations.

51 Although the most significant climate **impact** of eruptions are expressed over just
52 several years, they provide the source of the largest amplitude perturbations to Earth's
53 energy budget during the LM. For example, the eruption of Mt. Pinatubo in June 1991,
54 although transitory, exerted a radiative forcing comparable to an instantaneous halving of
55 atmospheric CO₂ [Hansen et al., 1992; Minnis et al., 1993; see also Driscoll et al. (2012)
56 for CMIP5 models]; several paleo-eruptions during the LM likely had an even larger
57 global impact (Figure 1).

58 One principal climate impact from volcanic eruptions results from the liberation
59 of sub-surface sulfur-containing gases such as sulfur dioxide (SO₂) and hydrogen sulfide
60 (H₂S), which are injected into the stratosphere and can react with water to form sulfate
61 (75% H₂SO₄) aerosols (e.g., Harshvardhan and Cess, 1976; Coakley and Grams, 1976;

62 Pollack et al., 1976, 1981; Lacis et al., 1992). The most pronounced impact of large
63 tropical eruptions includes a radiatively cooled troposphere and heated stratosphere (e.g.,
64 Lacis et al., 1992; Robock and Mao, 1995; Stenchikov et al., 1998). Sulfate aerosols from
65 the Mt. Pinatubo eruption had an effective radius of up to $\sim 0.5\text{-}0.8\ \mu\text{m}$, comparable in
66 size to a visible wavelength and strongly scattering to incoming solar radiation. Unless
67 the particles can reach sizes larger than $\sim 1\text{-}2\ \mu\text{m}$, this scattering more than offsets the
68 small increase in infrared opacity from the aerosols, and results in a cooling of Earth's
69 surface (Turco et al., 1982; Lacis et al., 1992). The stratospheric warming is caused by
70 absorption of near-infrared and longwave radiation, and results in anomalous temperature
71 gradients between the equator and poles, and an enhancement of the polar vortex. This
72 typically results in warming over sectors of the northern mid-latitudes during boreal
73 winter (e.g., Robock and Mao, 1992; Kirchner et al., 1999; Shindell et al., 2004;
74 Stenchikov et al., 2004; Stenchikov et al., 2006).

75 Studies on the impacts of volcanic eruptions have generally focused on global or
76 Northern Hemisphere metrics (e.g., Lucht et al., 2002; Gillett et al., 2004; Shindell et al.,
77 2004; Oman et al., 2005; Oman et al., 2006; Anchukaitis et al., 2010; Peng et al., 2010;
78 Evan et al., 2012; Zhang et al., 2013; Man et al., 2014), for instance in examining
79 responses to the East Asian monsoon system (EASM) or Arctic Oscillation.
80 Comparatively little attention has been given to the Southern Hemisphere, or to South
81 America specifically (although see Joseph and Zeng, 2011; and Wilmes et al., 2012).
82 Some previous work has focused on the Southern Annular Mode in the ERA-40 and
83 NCEP/NCAR reanalysis, in addition to a previous version of NASA GISS Model-E
84 (Robock et al., 2007) and in a subset of CMIP3 models (Karpechko et al., 2010) or in

85 CMIP5 (Gillett and Fyfe, 2013).

86 How volcanic forcing is expressed over South America remains an important
87 target question for several reasons. First, recognition of the South American monsoon
88 system (SAMS) as an actual monsoon system is less than two decades old (Zhou and
89 Lau, 1998), and thus study of SAMS dynamics is still relatively young (section 1.3) and
90 very little work has been done specifically focused on volcanic eruptions. For instance,
91 should we expect to see a reduction in austral summer rainfall (during the monsoon
92 season) as has been reported for the EASM (Man et al., 2014)? Secondly, the largest
93 volcanic eruptions during the late 20th century (e.g., Mt. Agung, 1963, Indonesia; El
94 Chichón, 1982, Mexico; Mt. Pinatubo, 1991, Island of Luzon in the Philippines-
95 hereafter, L20 eruptions) occur quasi-simultaneously with an anomalous El Niño-
96 Southern Oscillation (ENSO) state, thus limiting robust hypothesis-testing and guidance
97 for what impacts ought to be expected following large eruptions. Finally, South America
98 offers promise for a comparatively dense network of high-resolution proxy locations
99 relative to other tropical regions (see below), offering the potential to detect whether
100 South American hydroclimate signals to large eruptions are borne out paleoclimatically.

101 In this study, we will examine the post-volcanic response of South American
102 climate operating through the vehicle of unique model simulations (spanning the LM)
103 using the recently developed GISS ModelE2-R (LeGrande et al., 2014, in prep; Schmidt
104 et al., 2014a), which allows for the sampling of a greater number of events than is
105 possible over the instrumental period. Emphasis is placed on temperature and
106 precipitation, but a novel part of this study extends to the response of water isotopologues
107 in precipitation ($\delta^{18}\text{O}_p$, colloquially referred to hereafter as ‘isotopes’), since this is a key

108 variable that is directly derived from proxy data used in tropical paleoclimate
109 reconstructions.

110 The aim of this paper is to create a potentially falsifiable prediction for the
111 isotopic imprint that a volcanic eruption should tend to produce across the South
112 American continent. The ability to explicitly forward model the isotopic response allows
113 for a less ambiguous comparison of simulations and paleoclimate archives and for
114 hypothesis testing. It is unclear whether or not the current proxy archives are suitable to
115 test such a prediction given dating uncertainties, resolution, or the high level of noise in
116 proxy data. Additionally, the prevailing high-resolution archives in South America only
117 feature a few tropical records (Vimeux et al., 2009; Neukom and Gergis, 2012; Vuille et
118 al., 2012). Nonetheless, the growing number of high-resolution archives offers hope that
119 testing the modeled response to high-frequency volcanic signals will be an avenue for
120 future research. This can also better inform debate centered on the inverse problem in
121 interpreting isotopic signals (i.e., what do observed changes in proxy data imply about
122 past climate changes?), which remains contentious (section 1.4).

123 The structure of this article is as follows: in the remaining part of section 1, we
124 summarize previous literature on the impact of large volcanic eruptions on paleoclimate,
125 in addition to a discussion of South American climate. Section 2 presents data and
126 methodology, including how volcanic forcing is implemented in ModelE2-R. Section 3
127 discusses our results and we end with some conclusions in section 4.

128

129 1.2. Volcanic forcing during the Last Millennium

130

131 Volcanic forcing has had a very large influence on the climate of the LM
132 (Crowley, 2000; Hegerl et al., 2003; Shindell et al., 2004; Mann et al., 2005; Hegerl et
133 al., 2006; Fischer et al., 2007; D'Arrigo et al., 2009; Timmreck, 2012; Esper et al., 2013;
134 Ludlow et al., 2013; Schurer et al., 2014). Several studies (Miller et al., 2012; Schurer et
135 al., 2014) collectively provide a compelling case that volcanic forcing may be
136 substantially more important than solar forcing on a hemispheric-to-global scale during
137 the LM, in addition to driving a large portion of the inter-annual to multi-decadal
138 variability in LM simulations (Schmidt et al., 2014b).

139 For the LM, it is necessary to use measurements of the total acidity or the sulfate
140 content in ice cores for a reconstruction of the incidence of explosive volcanism (e.g.,
141 Hammer, 1980; Crowley et al., 1993; Robock and Free 1995; Zielinski et al., 1995;
142 Zielinski 2000). Anomalies in sulfur isotopes (via unique chemical processes in the
143 stratosphere causing mass-independent fractionation of the isotopes) can also be used to
144 distinguish between eruptions confined to the troposphere vs. those that inject large
145 quantities of material into the stratosphere (Savarino et al., 2003; Baroni et al., 2007;
146 2008). Two volcanic forcing datasets (Gao et al., 2008; Crowley and Unterman, 2013)
147 relying on ice core reconstructions of volcanism are used as input in the LM ModelE2-R
148 simulations, as discussed in Section 2.

149

150 1.3. South American Climate

151

152 South America is home to nearly 390 million people. The continent spans a vast
153 meridional extent (from ~10 °N to 55 °S), contains the world's largest rainforest (the

154 Amazon), in addition to a rather Mars-like desert (Atacama) that competes only with the
155 dry valleys of Antarctica for the driest location on Earth. The continent has diverse
156 orography, spanning the high Andes along the Pacific to Laguna del Carbón in Argentina,
157 the lowest point in the Southern Hemisphere. Because of this, South America hosts a rich
158 diversity of climate zones and biodiversity, all of which may respond in unique ways to
159 external forcing.

160 The most prominent climatic feature of tropical and subtropical South America is
161 the South American monsoon system (Zhou and Lau, 1998; Marengo et al., 2001; Vera et
162 al., 2006; Garreaud et al., 2009; Marengo et al., 2012). Much of South America is in a
163 monsoon regime, with tropical/subtropical rainfall over the continent exhibiting a
164 pronounced seasonal cycle. Unlike other monsoon systems such as that in Asia, low-level
165 easterly winds prevail during the entire year in tropical South America, **although the wind**
166 anomalies do change direction when the annual mean wind field is removed from winter
167 and summer composites (Zhou and Lau, 1998).

168 During austral winter, the maximum in continental precipitation is largely
169 restricted to north of the equator, in a band-like pattern associated with the oceanic Inter-
170 tropical Convergence Zone (ITCZ). During austral summer, convection is displaced from
171 northwestern South America, and a band of heavy precipitation covers much of the
172 continent, from the southern Amazon Basin to central Brazil and northern Argentina. A
173 distinctive feature of the SAMS is the South Atlantic Convergence Zone (SACZ), a band
174 of cloudiness and precipitation sourced primarily from the tropical Atlantic that extends
175 diagonally (southeastward) from the Amazon towards southeastern Brazil **(Figure 2)**.

176 The SAMS onset occurs around the end of October and the demise between the

177 end of March and April (e.g., Nogués-Paegle et al., 2002; Vera et al., 2006; Silva and
178 Carvalho, 2007). The dominant mode of intraseasonal precipitation variability over South
179 America during summer exhibits a dipole pattern (Nogués-Paegle and Mo, 1997),
180 seesawing between the SACZ region and Southeastern South America (SESA), the latter
181 including the densely populated La Plata basin with local economies strongly dependent
182 on agricultural activities.

183 The SAMS is strongly modulated by ENSO behavior on inter-annual timescales
184 (Vuille and Werner, 2005; Garreaud et al., 2009). In general, tropical South America
185 tends to experience drier than normal conditions during El Niño, while conditions in
186 subtropical latitudes are anomalously humid, including the southeastern part of the
187 continent. Surface air temperatures tend to be anomalously warm in tropical and
188 subtropical South America during El Niño events. These relationships depend somewhat
189 on the time of year, and during La Niña events, the pattern is essentially reversed.

190

191 1.4. Recent South American Monsoon reconstructions from isotopic proxies

192

193 SAMS variability spanning most of the Holocene has been diagnosed from
194 speleothem records in the Peruvian Andes (Kanner et al., 2013) and a review focused on
195 the last 1,000-2,000 years was given in Bird et al. (2011) and Vuille et al. (2012). In all
196 cases, a critical piece of information that is required to properly diagnose paleo-SAMS
197 variability is the ability to translate oxygen isotope variability from natural archives into a
198 physical climate signal of interest.

199 Early work on isotopes in ice core records from the tropical Andes detected a

200 Little Ice Age (LIA) signal in the oxygen isotope composition of the ice, with results
201 initially interpreted to reflect variations in local temperature due to their resemblance to
202 ice core records from Greenland (e.g., Thompson et al., 1995, 1998) and due to their
203 isotopic enrichment over the past 150 years, in parallel with rising global mean
204 temperatures (Thompson et al., 2006). A temperature-dependence to oxygen isotope
205 variability has been long known and is particularly important in mid-to-high latitudes
206 (Dansgaard, 1964) and is most directly related to the ratio of initial and final water vapor
207 content of a parcel that is transported horizontally, rather than the temperature-
208 dependence of fractionation itself (Hoffman and Heimann, 1997).

209 This interpretation in the tropics has been challenged through a number of
210 observational and modeling efforts (Hardy et al., 2003; Vuille and Werner 2005; Vimeux
211 et al., 2005, 2009; Kanner et al., 2012) which suggests that isotopes are much better
212 described as recording rainout upstream in regions of intense convection (in the case of
213 South America, over the Amazon basin). Additionally, since sea surface temperatures
214 (SST) in the Pacific have a large influence on SAMS intensity on inter-annual timescales
215 in the present, oxygen isotope variability over much of tropical South America is linked
216 to the state of the equatorial Pacific (Bradley et al., 2003; Vuille et al., 2003).

217 In regimes that are highly convective in nature as in tropical South America,
218 empirical evidence shows that the amount of precipitation (the so-called “amount effect”)
219 rather than the condensation temperature correlates most strongly with $\delta^{18}\text{O}$ variability, at
220 least on seasonal to inter-annual time scales. In reality, however, the rainout most
221 relevant for the oxygen isotope signal may be a significant distance from the site where
222 the proxy is derived, potentially complicating the use of local calibrations to climatology

223 as a guide for $\delta^{18}\text{O}$ interpretations (Schmidt et al., 2007). Isotopic concentrations are
224 explainable as being a function of original concentration, rainout along the moisture
225 transport path, and mixing.

226 **The influence of precipitation amount**, in addition to changes in the partitioning of
227 precipitation sources, has also been identified on decadal to orbital timescales through
228 speleothem records and lake sediments (Cruz et al., 2005; Van Breukelen et al., 2008;
229 Bird et al., 2011; Kanner et al., 2012). These studies have also highlighted the role of the
230 latitudinal displacement of the **Intertropical Convergence Zone (ITCZ)**, which is
231 ultimately the main moisture conduit for precipitation over the South American continent.
232 Furthermore, many records collected throughout South America now provide evidence
233 for enriched $\delta^{18}\text{O}$ values during the Medieval Climate Anomaly, which is indicative of
234 weakened SAMS convection and rainout, followed by depleted $\delta^{18}\text{O}$ values, suggesting
235 heavier rainfall during the LIA in tropical South America (Bird et al., 2011) with an
236 opposite response in Northeast Brazil (Novello et al., 2012). This, in turn, has been
237 interpreted in terms of North Atlantic SST anomalies (Vuille et al., 2012; Ledru et al.,
238 2013) and the position of the Atlantic ITCZ.

239 Nonetheless, **oxygen isotopes respond** in unique ways depending on the climate
240 forcing of interest. Indeed, a unique, quantitative local relationship between an isotope
241 record and any particular climate variable of interest is unlikely to hold for all timescales
242 and prospective forcing agents (Schmidt et al., 2007) thus motivating the use of forward
243 modeling to work in conjunction with proxy-based field data. For the remainder of this
244 paper, we focus specifically on the volcanic forcing response.

245

246 **2. Methodology**

247

248 2.1. Data

249

250 The primary tool used in this study is the water isotope-enabled **GISS** ModelE2-
251 R. ModelE2-R is a fully coupled atmosphere-ocean **GCM** (LeGrande et al 2014 in prep;
252 Schmidt et al., 2014a) that explicitly tracks stable water isotopes. The version used here
253 is the same as the **NINT** physics version used in the Coupled Model Intercomparison
254 Project Phase 5 (CMIP5) experiments. The current model features 2° latitude x 2.5°
255 longitude horizontal resolution and 40 vertical levels in the atmosphere up to 0.1 hPa, and
256 is coupled to the Russell Ocean that conserves heat, water mass, and salt (Russell et al.,
257 1995) at 1° x 1.25° resolution with 32 vertical levels. ModelE2-R includes stratospheric
258 dynamics and non-interactive ozone and aerosol species. Using a fully coupled model
259 offers the advantage of a more physically consistent simulation of the natural range of
260 climate variability and the interaction between different components of the climate
261 system, including ocean, atmosphere, and land.

262 Due to uncertainties in past radiative forcing, a suite of LM simulations using
263 ModelE2-R have been run with different combinations of plausible solar, volcanic, and
264 anthropogenic land use histories (Schmidt et al., 2011, 2012) but with identical
265 greenhouse gas and orbital evolution. These simulations span the period 850-2005 C.E.
266 There are two reconstructions of past volcanic activity (Gao et al., 2008; Crowley and
267 Unterman, 2013) that are used in the ModelE2 simulations. We focus only on results
268 from the Crowley reconstruction prior to 1850 CE due to a mis-scaling of the Gao forcing

269 in the model that roughly doubled the appropriate radiative forcing. For the historical
270 period (1850-present), the volcanic forcing history is based on Sato et al. (1993) and is
271 equivalent among the different simulation members.

272 For the LM, three forcing combinations are available in the GISS ModelE2-R
273 simulations that use the Crowley reconstruction for volcanic perturbations. These include
274 Pongratz et al. (2008) [land]/ Krivova et al. (2007) [solar], Kaplan et al (2010)
275 [land]/Krivova et al. (2007) [solar], and Pongratz et al. (2008) [land]/Steinhilber et al.
276 (2009) [solar] (see Schmidt et al., 2011, 2012).

277 Water isotope tracers are incorporated into the model's atmosphere, land surface,
278 sea ice, and ocean. These isotopes are advected and tracked through every stage of the
279 hydrologic cycle. At each phase change (including precipitation, evaporation, ice
280 formation or melting) an appropriate fractionation factor is applied (Schmidt et al., 2005)
281 and all freshwater fluxes are tagged isotopically.

282 Crowley and Unterman (2013) discuss the details behind the LM Aerosol Optical
283 Depth (AOD) reconstruction that defines the volcanic forcing time-series in ModelE2-R
284 (Figure 1). This estimate is derived from sulfate peaks in ice cores, which are relatively
285 well dated and referenced to the historical record during the satellite era. Crowley and
286 Unterman (2013) provide an AOD history over 4 latitude bands (from 0-30° and 30-90°
287 in both hemispheres). ModelE2-R uses a cubic spline to interpolate this forcing dataset
288 over 24 latitude bands. The choice of volcanic eruptions used for the LM analysis
289 (section 2.2 below) is based on the AOD dataset from this 24-latitude grid.

290 In addition to the model, we take advantage of the NASA GISS Surface
291 Temperature analysis (GISTEMP) land-ocean index (Hansen et al., 1999), and a merged

292 precipitation dataset using land gauges from 1948-1978 (Chen et al., 2002) and Global
293 Precipitation Climatology Project (GPCP) v2.1 from 1979-present that also incorporates
294 satellite data (Huffman et al., 2009). These datasets are called upon to gauge the spatial
295 pattern and tropical mean climate response following the most recent two L20 eruptions
296 (only land for Mt. Agung, since sufficient tropical precipitation coverage is not
297 obtainable before 1979).

298 The GPCP product offers considerably better global and South American
299 coverage than other precipitation datasets, although observational density for rainfall is
300 still considerably more problematic over South America than for many other regions of
301 the globe. There is a sharp drop-off in the number of rain gauge stations used in the
302 product prior to the 1950's over much of the South American continent. Figure S1 shows
303 the station density at the beginning month of each L20 eruption, and the total number of
304 stations over South America with time, in the Global Precipitation Climatology Centre
305 (GPCC) v6 gauge analysis (Schneider et al., 2013), a key input in the satellite-gauge
306 merged product.

307 Finally, in section 3.1 we present data from the Global Network of Isotopes in
308 Precipitation (GNIP) accessible from the International Atomic Energy Agency (IAEA)
309 for $\delta^{18}\text{O}_p$ as a test of the model's ability to track the seasonal hydrologic cycle in the form
310 of its isotopic response over South America before discussing the Last Millennium
311 results. Unfortunately, there is considerable spatial and temporal heterogeneity in the
312 GNIP data over South America, and no isotopic measuring station over the continent
313 exhibits the temporal continuity to assess the isotopic response to all three eruptions. In
314 fact, only a few stations have data overlap with one or two eruptions and with a sufficient

315 number of $\delta^{18}\text{O}_p$ data points to establish reasonable seasonal or annual statistics, ensuring
316 little hope that the prevailing network of observations is suitable for hypothesis testing in
317 our context. Because of this and the data drop-off in precipitation, we do not examine
318 observed South American hydroclimate responses to early 20th century eruptions.

319

320 2.2 Super-posed Epoch and Composite Analysis

321

322 For the most recent two L20 eruptions, we present a composited tropical-mean
323 (temperature and precipitation anomalies zonally averaged from 25°S to 25°N) super-
324 posed epoch analysis. The GISTEMP product already provides data in the form of
325 monthly anomalies, and the seasonal cycle was removed from the precipitation data at
326 each grid cell. Results for the super-posed epoch analysis are baselined such that the data
327 has zero mean during eight years from -3 to 5, with zero defining the eruption month of
328 El Chichón and Mt. Pinatubo. Mt. Agung is excluded in this analysis as it occurs before
329 1979.

330 Additionally, we present the spatial pattern of observed and simulated response
331 for temperature and precipitation for all three L20 eruptions. Results are shown for DJF
332 and JJA with two 3-month segments for each season included in the post-volcanic
333 response (e.g., Mt. Pinatubo erupted in June 1991, and so the JJA post-volcanic field is
334 shown for June-July-August 1991 and June-July-August 1992). The pre-eruption field
335 subtracted from this includes the five years prior to the eruption. Other sensible choices
336 for the non-eruption years (such as also using five years after the eruption or detrending
337 the dataset and using a 30 year climatology, not shown) do not significantly change the

338 results.

339 For the full LM spatial composites, eruptions are defined as points in which
340 vertically integrated (15 to 35 km) stratospheric AOD averaged from 20°N to 30°S
341 exceeds 0.1 for at least 12 consecutive months in the simulation (top panel in Figure 1);
342 this criterion yields 16 eruptions since 850 C.E. The selection of events used in the LM
343 composite is very weakly sensitive to the choice of latitude band. A notable exception is
344 El Chichón that was used in the L20 composites, but not for the LM, since this event is a
345 “unipolar” eruption (Crowley and Unterman, 2013) in the sense that the largest AOD
346 perturbation is confined to the Northern Hemisphere despite the eruption being of tropical
347 origin. Mt. Agung and Mt. Pinatubo are actually the first and second smallest eruptions in
348 this selection based on the maximum AOD encountered near the time of the eruption (see
349 Table 1 for dates of each event).

350 For the LM “non-eruption” fields used to define the anomaly for each event,
351 months for 15 years on either side of each eruption are used, not including months in
352 which the AOD exceeds 0.1, either for that eruption or any overlapping months from
353 other eruptions (overlap occurs only once for eruptions in 1809 and 1815). When
354 constructing seasonal averages of $\delta^{18}\text{O}_p$ in the model, the oxygen isotope value for each
355 month is weighted by the precipitation amount during that month, at each grid cell.

356 Since each post-eruption difference field is computed using the immediate
357 response minus a surrounding 30-year climatology, time is not relevant in this analysis
358 and so we use all three ensemble members with the Crowley forcing to generate a
359 composite that features 48 volcanic “events” (16 eruptions in each of the 3 members).

360 For the model composites covering the L20 eruptions, the mis-scaling of the Gao forcing

361 is not an issue, and so we use six ensemble members each. The ensemble-mean
362 composite results displayed for the LM/L20 eruptions include contributions from
363 three/six members which differ not just in the internal variability, but also differences due
364 to solar and land-use forcing. However, the primary signal of interest only lasts for a few
365 years following an eruption and is expected to be large compared to the impact of more
366 slowly varying and smaller-amplitude forcings. Therefore, the ensemble spread to a given
367 eruption can be interpreted as a sampling of the model internal variability coincident with
368 the event.

369 Finally, it is now well appreciated that any climate response under investigation
370 will be slaved to the spatial structure of the forcing imposed on a model. For example,
371 preferential heating/cooling of one hemisphere will induce different tropical precipitation
372 responses than a well-mixed gas that behaves CO₂-like (Kang et al., 2008, 2009; Frierson
373 and Hwang, 2012; Haywood et al., 2012). Figures S2 and S3 show the latitudinal AOD
374 distribution structure for all eruptions used in the generation of the LM composites within
375 ModelE2-R. The mean of all events is rather symmetric between hemispheres (though
376 somewhat skewed toward the Southern Hemisphere tropics, which is linked to the
377 selection criteria), and similar to the pattern expected with CO₂ change, the forcing is
378 largest in the tropics. Thus, the resulting climate responses outlined in this paper ought to
379 be viewed as a response consistent with a forcing that is symmetric about the equator. We
380 plan to further explore the influence of location in a separate paper.

381

382 2.3. Influence of ENSO on the Late 20th Century (L20) eruptions

383

384 For all three volcanic events during the last 60 years, El Niño events are occurring
385 quasi-simultaneously with the eruption. This introduces a pervasive issue when
386 attempting to isolate the volcanic signal (e.g., Robock, 2003; Trenberth and Dai, 2007;
387 Joseph and Zeng, 2011) and is particularly important over South America (e.g. Garreaud
388 et al., 2009).

389 In order to remove the effects of ENSO from the super-posed epoch and spatial
390 composite analyses described above in the GISTEMP and GPCP data, we first perform a
391 multiple regression with the variable of interest over the period 1951-2005 using a linear
392 time trend and the Niño 3 index as predictors (5°N-5°S, 150°W -90°W, data from
393 <http://www.cpc.ncep.noaa.gov/data/indices/>) over the same period, excluding two years
394 of data after each L20 eruption. At each grid cell, the Niño 3 index is lagged from 0-6
395 months and the correlation coefficient with the maximum absolute value (since a positive
396 index can induce a negative anomaly in the variable of interest) is found. This is similar
397 to the approach used in Joseph and Zeng (2011), allowing the maximum ENSO influence
398 to be removed at each grid point at different times. The lagged Niño index is then
399 regressed against the time series of each variable and the residual from this regression is
400 retained. This approach assumes a linear relationship between ENSO and the climate
401 response over South America, an assumption that appears justified on inter-annual to
402 decadal time scales (Garreaud et al., 2009).

403 For each of the six ensemble members used in the model L20 composite, a similar
404 procedure is performed in which the Niño 3 index (consistent with the realization of the
405 Niño 3 domain SSTs in that model simulation) is calculated and regressed out in the same
406 manner. For the full LM computations, the large number of events in the three-ensemble

407 member composite should help average out the influence of Pacific SST variability, and
408 no ENSO removal procedure is applied.

409

410 **3. Results and Discussion**

411

412 3.1. L20

413

414 Figures 3a and b show the ENSO-removed super-posed epoch analysis for
415 tropical temperature and precipitation associated with the recent two L20 eruptions. Both
416 time-series series exhibit negative anomalies in the composite, although the precipitation
417 response is noisier. There is good agreement between the observed and modeled
418 temperature response, both in amplitude and recovery timescale. The precipitation signal
419 displays a modest reduction in the composite, with the recovery in observations occurring
420 faster (between year 1 and 2) than in the model, although this behavior emerges from a
421 different recovery pattern between El Chichón and Mt. Pinatubo (not shown). The peak
422 monthly precipitation reduction is larger in both the observations and model for Mt.
423 Pinatubo, consistent with a larger AOD perturbation.

424 The spatial structure of the late 20th century temperature and precipitation
425 response for both solstice seasons in observations and the model (ensemble mean) are
426 shown in Figures 4 and 5, respectively. Observations exhibit cooling over much of the
427 globe, especially after Mt. Pinatubo that is largely reproduced by the model. The model
428 results are averaged over six ensemble members reducing the amplitude of some of the
429 structure seen in observations, although many of the patterns observed are also borne out

430 in the simulations. For instance, the JJA temperature expression over the United States is
431 reproduced as a cooling after El Chichón and Mt. Pinatubo, with a warm anomaly in the
432 middle and eastern part of the continent following Mt. Agung in both the model and
433 observations. A wave-like dynamic warm pattern (discussed in section 1.1) is observed
434 during DJF in northern mid-latitudes, a pattern recovered in ModelE2-R. Widespread
435 tropical African cooling is observed after Mt. Pinatubo in both seasons, and after El
436 Chichón during boreal winter.

437 **In GISTEMP**, the high-latitudes of South America cool more than the tropical
438 region of the continent for all observed cases except El Chichón during the DJF season, a
439 pattern not reproduced by the model simulations. The largest differences often relate to
440 the state of the Pacific. For example, there is a residual signal from ENSO following El
441 Chichón that is not reproduced by the model. This would not be expected in a free-
442 running coupled simulation. The magnitude of this signal is sensitive to the Niño index
443 used in the regression method described above. Performing a regression procedure using
444 other ENSO indices such as SST anomalies from the Niño 3.4 domain, Cold Tongue
445 Index, or Multivariate Enso Index do not perform better in removing the East Pacific SST
446 residual after El Chichón, although the linear regression approach performs well at
447 removing ENSO signatures over the South American continent. With no ENSO removal
448 procedure applied this East Pacific warm anomaly is much stronger following El Chichón
449 and becomes very apparent after Mt. Pinatubo as well, with relatively warm SSTs
450 spanning nearly the entire tropical Pacific. Additionally, without ENSO removal, tropical
451 South America warms following the two eruptions (not shown). The influence of ENSO
452 appears minimal over the higher latitude sectors of the continent. Thus the comparison to

453 the model in the South American tropics is connected to the ENSO state and the removal
454 procedure employed.

455 The precipitation pattern after all three L20 eruptions exhibits substantial
456 variability in space and across eruptions, with a general drying pattern over land in
457 tropical latitudes and further evidence of imperfect ENSO removal procedure in the
458 Pacific ocean. South America tends to experience less precipitation near the equator
459 during austral winter, although the model mean produces increased rainfall following El
460 Chichón. There is a dipole structure in the observed response during for the first two L20
461 eruptions not captured in the model, although there is considerable spread among each
462 members in the generated composite (not shown).

463 Figure 6 illustrates that ModelE2-R reproduces the seasonal cycle of
464 climatological rainfall (contoured) and oxygen isotope distribution (color) with some
465 fidelity over South America. Where data **permits** (Figure 6a) there is good agreement
466 between the spatial structure of oxygen isotope DJF enrichment relative to JJA (near the
467 equator and over the continent in the Northern Hemisphere, and in the higher latitudes
468 south of 30°S), and depletion in the continental interior associated with the wet season.
469 ModelE2-R (Figure 6b) **tends to produce too much DJF precipitation in far eastern Brazil**
470 although the seasonal migration of rainfall is well captured. This agreement has also been
471 noted in two atmospheric GCMs with no coupled ocean (NASA-GISS II and ECHAM-4,
472 see Vuille et al., 2003).

473 Because of the considerable variability seen in observations and also across
474 ensemble members, it is evident that a larger signal-to-noise ratio is required to help
475 isolate any volcanic signal. ModelE2-R is the laboratory from which we proceed to

476 sample a larger number of events, some of which contain larger amplitude than the L20
477 eruptions.

478

479 3.2. Last Millennium Composites

480

481 *a. Temperature and Precipitation*

482

483 Figure 7 shows the LM post-volcanic temperature composite for all 48 events.
484 During both seasons, cooling is statistically significant over virtually the entire continent
485 (all spatial composites for the LM events are masked for significance at the 90% level
486 using a two-sided student t-test). The temperature response is strongest in the interior of
487 the continent, particularly during the austral winter. The enhanced high-latitude cooling
488 exhibited in the observations does not emerge in the model composite.

489 The precipitation anomalies for the LM composite are shown in Figure 8. As
490 expected, there is a distinct seasonal structure in the response, with the anomaly
491 concentrated in a narrow region north of the equator during austral winter. During JJA,
492 precipitation increases in the North Atlantic region at the expense of a very strong and
493 statistically significant precipitation reduction over the equator (including Northern
494 Brazil, Ecuador, Venezuela, Colombia, and Guyana) and encompassing the northern
495 Amazon Basin. This signal is consistent with a locally displaced ITCZ and a general
496 weakening of the moisture flux owing to the decrease in saturation vapor pressure due to
497 cooling that is demanded by Clausius-Clapeyron (Held and Soden, 2006). During this
498 season, the precipitation response is significant virtually everywhere in northern South

499 America. Supplementary Figure (S5) further illustrates that the JJA precipitation response
500 is remarkably robust to all eruptions that enter into the composite.

501 Figure 9b illustrates the relationship between area-averaged precipitation from
502 20°S- 0° (DJF) and 0° to 12°N (JJA, these different regions were selected to reflect the
503 seasonal migration of rainfall) and the maximum AOD encountered for each eruption. 16
504 eruptions are displayed with the three-member ensemble spread given for each. All data
505 is zonally averaged from 75°W to 45°W. Precipitation only increases north of the equator
506 during austral winter in a few model realizations. Moreover, the magnitude of the
507 precipitation response during JJA scales with the size of the eruption, particularly for
508 very large eruptions (e.g., comparing five eruptions with AOD > 0.3 vs. those with
509 smaller perturbations, although the spread amongst the ensemble members is large). The
510 spatial composite for each individual eruption (each averaged over the three ensemble
511 members) is shown in Figure S5.

512 The precipitation response during austral summer is more difficult to interpret
513 (Figure 8a). During this season, the zonally oriented Atlantic ITCZ migrates southward
514 and the SACZ becomes more intense as it is connected with the area of convection over
515 the central and southeastern part of the continent. It is noteworthy that the land cools
516 substantially more than the surrounding ocean (Figure 7), which one could expect to
517 weaken the monsoon-sourced precipitation during DJF. While precipitation is indeed
518 reduced over the tropical continent, the response is weaker than in JJA and less spatially
519 coherent, with many areas failing to meet statistical significance. An analysis of the
520 individual responses reveals that the signal is more eruption-dependent during DJF than
521 during JJA (see Figure S4), with a few events actually exhibiting modest increases in

522 precipitation. Nonetheless, there is a clear tendency for reduced DJF precipitation within
523 the SAMS region, although there is little to no dependence of the mean rainfall anomaly
524 on the magnitude of the AOD perturbation, at least above the 0.1 threshold used in this
525 study (Figure 9b), unlike for equatorial South America during JJA. Conversely, the
526 temperature response in the SAMS domain (for DJF) (Figure 9a) depends on the size of
527 the eruption, as is expected.

528

529 *b. Tropical Hydrological Cycle response*

530

531 Since the South American climate is intimately linked to large-scale tropical
532 dynamics, the global precipitation composite is shown in Figure S6 to better inform the
533 model response. The most robust signal is for a reduction in tropically averaged
534 precipitation and the tendency for wet regions to become drier, and dry regions to
535 become wetter (see also Iles et al., 2013), in contrast to the anticipated hydrologic
536 response in a future, higher-CO₂ world (Held and Soden, 2006).

537 This pattern is a thermodynamic effect linked to reduced moisture convergence
538 within the convergence zones and to reduced moisture divergence in the descending
539 zones of the Hadley cell, which reduces the contrast in values of precipitation minus
540 evaporation (P-E) between moisture convergence and divergence regions (Chou et al.,
541 2009). The complete hydrologic response of the $\Delta P-E$ field (not shown) has the same
542 spatial structure as the ΔP field, since evaporation is decreasing nearly everywhere in the
543 tropics. Because both P and E are decreasing on the equator-ward flank of the ITCZ the

544 ΔP -E signal is rather weak in the deep tropics, while ΔP -E increases more rapidly than ΔP
545 in the subtropics.

546 The tendency for modest precipitation anomalies over the continent during DJF
547 appears to be part of a pattern that spans a broad swath of longitudes across the entire
548 deep tropics in association with the seasonal cycle. Nonetheless, the response over DJF is
549 weaker over land. However, land hydrologic responses that are only weakly sensitive to
550 anomalies over the ocean can be expected (Greve et al., 2014).

551

552 *c. Oxygen Isotope Anomalies*

553

554 In order to relate the responses discussed in the previous sections back to a
555 potentially observable paleoclimate metric, we show the composite $\Delta\delta^{18}O_p$ field for the
556 DJF and JJA seasons in South America (Figure 10). It should be cautioned that much of
557 the isotopic variability that can be observed in proxies within the continental interior or
558 high-elevation glacier sites will likely be seasonally biased toward the wet season months
559 (Hardy et al., 2003).

560 During the JJA season, there is a strong enrichment of the $\delta^{18}O_p$ pattern that is
561 zonally extended over equatorial South America. In addition, there is a corresponding
562 $\delta^{18}O_p$ depletion in the adjacent North Atlantic sector. This response is inextricably
563 coincident with the strong change in precipitation in the ITCZ domain that was assessed
564 in Figure 8, and is broadly consistent with a “rainfall amount” control on the isotopic
565 imprint (Dansgaard, 1964). South of approximately 15°S, the sign of the anomaly
566 reverses to a depletion of the heavy isotope.

567 During the austral summer, volcanic eruptions lead to a clear negative excursion
568 in $\delta^{18}\text{O}_p$ over virtually the entire SAMS region, including the Amazon basin, tropical
569 Andes, and eastern Brazil. The statistical significance of the resulting isotopic anomaly
570 extends throughout most of the landmass within the tropics and in the North Atlantic.
571 There are small but non-significant exceptions (positive $\delta^{18}\text{O}_p$ excursions) such as in
572 eastern Brazil. The negative excursions also include regions outside of the SAMS belt in
573 the subtropics and mid-high latitudes of South America.

574 Remarkably, the austral summer $\delta^{18}\text{O}_p$ depletion is the opposite sign from what
575 one would expect if the reduced precipitation were driving the isotopic response. Thus, it
576 may well be that the strong temperature response to volcanic eruptions dominates the
577 continent-wide oxygen isotope depletion during the DJF season and in the extratropics
578 during JJA over the relatively weak precipitation response. Precipitation on the other
579 hand appears to be the primary control knob of $\delta^{18}\text{O}_p$ during JJA within the ITCZ region.

580 In the case of volcanic forcing it appears that the amplitude of the temperature-
581 response to volcanic eruptions over tropical South America is much larger than the rather
582 weak and spatially incoherent precipitation signal. This may explain why the isotopic
583 signal related to volcanic eruptions seems to respond primarily to atmospheric cooling,
584 even in the tropics, where isotopic variability is usually more closely associated with
585 changes in the hydrologic cycle.

586 Taken together, these results suggest that the primary controls on oxygen isotope
587 variability are forcing and event-dependent, rather than being determined inherently by
588 the latitude of interest (e.g., “precipitation driven” in the tropics and “temperature driven”
589 in the extratropics as is often assumed). This conclusion is compelled by the fact that the

590 precipitation production and distribution in proxy records are the result of an interaction
591 between multiple scales of motion in the atmosphere, the temperature of air in which the
592 condensate was embedded, and exchange processes operating from source to sink of the
593 parcel deposited at a site. Thus, a consistent description of how to interpret oxygen
594 isotopes into a useful climate signal cannot be given without considering all of these
595 processes and the target process of interest.

596 To further complement the spatial analysis, a composite Hovmöller diagram is
597 utilized (Figure 11) in order to illustrate the time-evolution of the temperature,
598 precipitation, and oxygen isotope response. For this plot, the start of each eruption is
599 defined as the closest January to the first month in which AOD reaches 0.1 in order to
600 illustrate the seasonal evolution (rather than compositing by “month from each eruption”
601 as in Figure 3). Therefore, for all 48 events in the composite, the local AOD may reach
602 this threshold within five months (before or after) of the January baseline point (eruptions
603 in June are rounded up to the following January). The Hovmöller composites are plotted
604 for ten years (beginning January three years prior to the eruption). The closest January
605 point to the start of each eruption occurs in the 37th month of the Hovmöller (solid black
606 line in Figure 11a,b,d). Results are zonally averaged from 75° to 45° W, across the
607 SAMS region.

608 Figure 11a demonstrates a substantial temperature anomaly that peaks south of
609 10°S (compare also to Figure 7). The cooling lasts for several years following the
610 eruption, and decays until much of the signal is lost (~4 years after the eruption at all
611 latitudes). The zonally averaged peak reductions in South American precipitation
612 anomalies occur over the tropical latitudes and last for a comparable period of time as the

613 temperature response. The precipitation anomaly itself migrates synchronously with the
614 seasonal cycle (red line in Figure 11c maps out the latitude of maximum climatological
615 precipitation averaged over all 30 year climatologies of each 48-member event, as a
616 function of time of year). Figure 11b indicates that the largest precipitation response is
617 confined to the equatorial regions during JJA, and any protrusion into mid-latitudes (still
618 equatorward of the storm track), although weaker in magnitude, only occurs during the
619 summer.

620 Figure 12 provides additional statistical insight into the magnitude of the
621 excursions described in this section. Here, we sampled 100 random 48-event composites
622 in a control simulation with no external forcing (each “event” two seasons in length
623 defined as an anomaly expressed relative to a surrounding climatology as done
624 previously). The anomalies were averaged over the same areas as in Figure 9, with
625 different domains for DJF and JJA. Notably, for both seasons and for all three variables
626 examined, the single 48-event post-volcanic composite (red line) lies outside the
627 distribution of all sampled 48-event composites constructed with no external forcing.
628 Nonetheless, the distribution for a smaller sample of events (grey solid line denotes the
629 normal distribution with the mean and standard deviation from the data of 16 eruptions
630 each averaged over the three ensemble members) shows considerable spread.

631

632 *d. Dynamics and Extratropical & High-Latitude Influence*

633

634 A number of studies have discussed the impact of volcanic forcing on high-
635 latitude Southern Hemisphere dynamics (e.g., Robock et al., 2007; Karpechko et al.,

636 2010; Wilmes et al., 2012; Gillett and Fyfe, 2013) with several potential consequences
637 for South America. Like the ITCZ, the SACZ in particular is quite capable of exhibiting
638 meridional displacements in response to external forcing. For example, Gonzalez et al.
639 (2013) attributed a significant 20th century wetting trend in the SESA region during DJF
640 to ozone forcing, supporting the notion of polar-driven changes in the subtropics (Kang et
641 al., 2011). A similar trend may arise in the future if the SACZ moves poleward in concert
642 with the large-scale circulation (Seth et al., 2010).

643 During the austral summer, Figure 13 indicates a tendency for ModelE2-R to
644 redistribute atmospheric mass toward higher latitudes during DJF and over the south
645 Atlantic sector near South America during JJA. This pattern somewhat resembles the
646 negative phase of the Southern Annular mode (SAM), although it exhibits a tripole
647 structure and relatively weak signals in regions particularly important for SACZ
648 dynamics. The precipitation anomalies spanning from the Southern Ocean to South
649 America form a band-like pattern (not shown) that is anti-correlated with the sea level
650 pressure signal although the direct impact of this extratropical influence appears rather
651 modest over the South American continent. Additionally, the tropical easterlies from the
652 North Atlantic that act as a conduit for moisture transport toward South America also
653 decrease in magnitude. The weakened moisture transport coupled with the
654 thermodynamic effect of a cooler, drier atmosphere may explain the tendency for
655 precipitation reductions over eastern Brazil and parts of the Amazon basin in most of the
656 eruption events (Figure S4) and in the LM composites, but there is no evidence for any
657 substantial change in the dynamics that would change the source region for moisture and
658 dominate the oxygen isotope excursions.

659

660 *e. Land Surface Hydrologic Response*

661

662 An important component of South America's hydrologic cycle, and potentially
663 the interpretation of oxygen isotope anomalies left behind in natural archives, are local
664 land-surface hydrology feedbacks and water recycling efficiency over the continent.

665 Figure 14 shows that land evaporation and river discharge decrease throughout tropical
666 South America in the post-volcanic composite. The runoff anomalies are particularly
667 pronounced over the Amazon River drainage basin and the Orinoco River in Venezuela
668 and Colombia. The modeled oxygen isotope response at the surface (not shown) is very
669 well correlated with the $\delta^{18}\text{O}_p$ signal, though these responses may be of interest to
670 hydrologists studying in the Amazon Basin.

671

672 **4. Conclusions**

673

674 In this study, we have summarized the response of temperature, precipitation, and
675 $\delta^{18}\text{O}_p$ to volcanic forcing for the L20 historical set of events, in addition to many large
676 eruptions during the Last Millennium. It is now well known that volcanic eruptions lead
677 to large-scale cooling throughout the tropics, and this result extends to most of the South
678 American continent as well, except in regions that may be simultaneously affected by
679 opposing ENSO behavior. In general, the precipitation response has been more
680 enigmatic, though our results are in broad agreement with numerous other studies that
681 there is a substantial decline in tropical-mean precipitation.

682 However, the immediate post-volcanic impact over South America has a complex
683 seasonal and spatial structure. During the austral winter, the precipitation response over
684 the continent is slaved to the response of the large-scale circulation, including a
685 weakening of rainfall intensity within the ITCZ that is migrating northward. In the
686 extratropics, the continent cools and exhibits slight precipitation declines nearly
687 everywhere. Our results suggest the seasonal monsoon precipitation (during DJF) in
688 ModelE2-R exhibits a fairly weak response that is scattered across the continent. It
689 appears that volcanic forcing preconditions the tropical rainfall over the continent to
690 decline during the wet season, but that this response is likely to be eruption-dependent
691 and may be overwhelmed by internal variability.

692 A unique aspect of this study was to probe the $\delta^{18}\text{O}_p$ response to volcanic
693 eruptions. During JJA, isotopes become heavily enriched in northern South America as
694 convective activity produces substantially less precipitation. No such relation was found
695 during the monsoon season, even within the tropics, where the large cooling appears to
696 lead to more depleted $\delta^{18}\text{O}_p$, despite a weakened hydrologic cycle and reduced monsoon
697 precipitation. In the extratropics, it appears that the temperature decline is driving
698 isotopes toward more depleted values.

699 Unfortunately validation of our model results is hindered by the paucity of
700 observational stable isotope data and by the coincidence of volcanic eruptions with
701 ENSO events over the 20th century. Nonetheless our results may provide some guidance
702 in the search of volcanic signals in high-resolution isotopic proxy data from South
703 America. Given the importance of volcanic forcing for climate variability over the past
704 millennium, and in particular the LIA period, which has been identified as a period of

705 significant climatic perturbation in isotopic proxies from South America, a better
706 understanding of the climatic response to volcanic forcing over this region is urgently
707 needed.

708

709

710 *Acknowledgments:*

711 This study was funded by NOAA C2D2 NA10OAR4310126 and NSF awards
712 AGS-1003690 and AGS-1303828. We would like to thank NASA GISS for institutional
713 support; resources supporting this work were provided by the NASA High-End
714 Computing (HEC) Program through the NASA Center for Climate Simulation (NCCS) at
715 Goddard Space Flight Center. We are grateful for the insightful comments of three
716 anonymous reviewers, which helped us to significantly improve the manuscript

717

718

719

720

721

722

723

724

725

726

727

728

729 **References**

730

- 731 Anchukaitis, K.J., B.M. Buckley, E.R. Cook, B.I. Cook, R.D. D'Arrigo, and C.M.
732 Ammann, 2010: The influence of volcanic eruptions on the climate of the Asian
733 monsoon region. *Geophys. Res. Lett.*, **37**, L22703.
- 734 Baroni M., M.H. Thiemens, R.J. Delmas, and J. Savarino, 2007: Mass-independent
735 sulfur isotopic compositions in stratospheric volcanic eruptions, *Science*, **315**, 84–87.
- 736 Baroni, M., J. Savarino, J. Cole-Dai, V.K. Rai, and M.H. Thiemens, 2008: Anomalous
737 sulfur isotope compositions of volcanic sulfate over the last millennium in Antarctic
738 ice cores, *J. Geophys. Res.*, **113**, D20112.
- 739 Bird, B.W., M.B. Abbott, D.T. Rodbell, and M. Vuille, 2011: Holocene tropical South
740 American hydroclimate revealed from a decadal resolved lake sediment $\delta^{18}\text{O}$
741 record, *Earth Planet. Sci. Lett.*, **310**, 192-202.
- 742 Bradley, R.S., M. Vuille, D.R. Hardy, and L.G. Thompson, 2003: Low latitude ice cores
743 record Pacific sea surface temperatures, *Geophys. Res. Lett.*, **30**, 1174.
- 744 Chen, M., P. Xie, J. E. Janowiak, and P. A. Arkin, 2002: Global Land Precipitation: A
745 50-yr Monthly Analysis Based on Gauge Observations. *J. Hydrometeor*, **3**, 249–266.
- 746 Chou, C., J.D. Neelin, C.-A. Chen, and J.-Y. Tu, 2009: Evaluating the “Rich-Get-
747 Richer” Mechanism in Tropical Precipitation Change under Global Warming. *J.*
748 *Climate*, **22**, 1982–2005.

749 Coakley, J.A., and G.W. Grams, 1976: Relative Influence of Visible and Infrared
750 Optical Properties of a Stratospheric Aerosol Layer on the Global Climate. *J. Appl.*
751 *Meteor.*, **15**, 679–691.

752 Cole-Dai, J., 2010: Volcanoes and climate, *Wiley Interdisciplinary Reviews: Climate*
753 *Change*, **1**, 824-839.

754 Crowley, T.J., T.A. Christe, and N.R. Smith, 1993: Reassessment of Crete (Greenland)
755 ice core acidity/volcanism link to climate change, *Geophys. Res. Lett.*, **20**, 209–212.

756 Crowley, T.J., 2000: Causes of climate change over the past 1000 years, *Science*, **289**,
757 270–277.

758 Crowley, T. J. and M.B. Unterman, 2013: Technical details concerning development of
759 a 1200-yr proxy index for global volcanism. *Earth Syst. Sci. Data*, **5**, 187–197.

760 Cruz, F.W., S.J. Burns, I. Karmann, W.D Sharp, M. Vuille, A.O. Cardoso, J.A. Ferrari,
761 P.L.S. Dias, and O. Viana, 2005: Insolation-driven changes in atmospheric circulation
762 over the past 116,000 years in subtropical Brazil, *Nature*, **434**, 63-66.

763 Dansgaard, W., 1964: Stable isotopes in precipitation. *Tellus*, **16**, 436–468.

764 D'Arrigo, R., R. Wilson, and A. Tudhope, 2009: The impact of volcanic forcing on
765 tropical temperatures during the past four centuries. *Nature Geosci.*, **2**, 51–56.

766 Driscoll, S., A. Bozzo, L.J. Gray, A. Robock, and G. Stenchikov, 2012: Coupled Model
767 Intercomparison Project 5 (CMIP5) simulations of climate following volcanic
768 eruptions. *J. Geophys. Res.*, **117**, D17105.

769 Emile-Geay, J., R. Seager, M.A. Cane, E.R. Cook, and G.H. Haug, 2008: Volcanoes and
770 ENSO over the Past Millennium, *J. Climate*, **21**, 3134–3148.

771 Esper J., L. Schneider, P.J. Krusic, J. Luterbacher, U. Büntgen, M. Timonen, F. Sirocko
772 and E. Zorita, 2013: European summer temperature response to annually dated
773 volcanic eruptions over the past nine centuries. *B. Volcanol.* **75**, 1-14.

774 Evan, A.T., 2012: Atlantic hurricane activity following two major volcanic eruptions, *J.*
775 *Geophys. Res.*, **117**, D06101.

776 Fischer, E.M., J. Luterbacher, E. Zorita, S.F.B. Tett, C. Casty, and H. Wanner, 2007:
777 European climate response to tropical volcanic eruptions over the last half
778 millennium, *Geophys. Res. Lett.*, **34**, L05707.

779 Frierson, D.M.W., and Y. Hwang, 2012: Extratropical Influence on ITCZ Shifts in Slab
780 Ocean Simulations of Global Warming. *J. Climate*, **25**, 720–733.

781 Gao, C., A. Robock, and C. Ammann, 2008: Volcanic forcing of climate over the past
782 1500 years: an improved ice core-based index for climate models, *J. Geophys. Res.*,
783 **113**, D23111.

784 Garreaud, R.D., M. Vuille, R. Compagnucci, and J. Marengo, 2009: Present-day South
785 American climate, *Palaeogeogr. Palaeoclimatol. Palaeoecol.*, **281**, 180-195.

786 Gillett, N.P., A. J. Weaver, F. W. Zwiers, and M. F. Wehner, 2004: Detection of volcanic
787 influence on global precipitation, *Geophys. Res. Lett.*, **31**, L12217.

788 Gillett, N.P., and J.C. Fyfe, 2013: Annular mode changes in the CMIP5 simulations,
789 *Geophys. Res. Lett.*, **40**, 1189–1193.

790 Gonzalez, P.L.M., L.M. Polvani, R. Seager, and G.J.P. Correa 2013: Stratospheric ozone
791 depletion: a key driver of recent precipitation trends in South Eastern South America.
792 *Climate Dyn.* 1-18.

793 Goosse, H., T. Crowley, E. Zorita, C. Ammann, H. Renssen, and E. Driesschaert, 2005:
794 Modelling the climate of the last millennium: what causes the differences between
795 simulations? *Geophys. Res. Lett.*, **32**, L06710.

796 Greve P., B. Orlowsky B, B. Mueller, J. Sheffield, M. Reichstein, and S.I. Seneviratne,
797 2014: Global assessment of trends in wetting and drying over land, *Nature Geosci.*, **7**,
798 716-721.

799 Hammer, C.U., H.B. Clausen, and W. Dansgaard 1980: Greenland ice sheet evidence of
800 post-glacial volcanism and its climatic impact. *Nature*, **288**, 230–235.

801 Hansen, J., A. Lacis, R. Ruedy, and M. Sato, 1992: Potential climate impact of Mount
802 Pinatubo eruption, *Geophys. Res. Lett.*, **19**, 215-218.

803 Hansen, J., R. Ruedy, J. Glascoe, and M. Sato, 1999: GISS analysis of surface
804 temperature change. *J. Geophys. Res.*, **104**, 30997-31022.

805 Hardy, D.R., M. Vuille, and R.S. Bradley, 2003: Variability of snow accumulation and
806 isotopic composition on Nevado Sajama, Bolivia. *J. Geophys. Res.*, **108**, 4693.

807 Harshvardhan, and R.D. Cess, 1976: Stratospheric aerosols: effect upon atmospheric
808 temperature and global climate. *Tellus*, **28**, 1-10.

809 Haywood, J.M., A. Jones, N. Bellouin, and D. Stephenson, 2013: Asymmetric forcing
810 from stratospheric aerosols impacts Sahelian rainfall. *Nature Climate Change*, **3**, 660-
811 665.

812 Hegerl, G.C., T.J. Crowley, S.K. Baum, K.Y. Kim, and W.T. Hyde, 2003: Detection of
813 volcanic, solar and greenhouse gas signals in paleo-reconstructions of Northern
814 Hemispheric temperature, *Geophys. Res. Lett.*, **30**, 1242.

815 Hegerl, G.C., T.J. Crowley, W.T. Hyde, and D.J. Frame, 2006: Climate sensitivity

816 constrained by temperature reconstructions over the past seven centuries. *Nature*,
817 **440**, 1029–1032.

818 Held, I.M., and B.J. Soden, 2006: Robust Responses of the Hydrological Cycle to Global
819 Warming. *J. Climate*, **19**, 5686–5699.

820 Hoffmann, G., and M. Heimann, 1997: Water isotope modeling in the Asian monsoon
821 region. *Quat. Inter.*, **37**, 115–128.

822 Huffman, G. J., R. F. Adler, D. T. Bolvin, and G. Gu, 2009: Improving the global
823 precipitation record: GPCP Version 2.1, *Geophys. Res. Lett.*, **36**, L17808.

824 Iles, C.E., G.C. Hegerl, A.P. Schurer, and X. Zhang, 2013: The effect of volcanic
825 eruptions on global precipitation, *J. Geophys. Res. Atmos.*, **118**, 8770–8786.

826 Joseph, R., and N. Zeng, 2011: Seasonally Modulated Tropical Drought Induced by
827 Volcanic Aerosol. *J. Climate*, **24**, 2045–2060.

828 Kang, S.M., I.M. Held, D.M.W. Frierson, and M. Zhao, 2008: The Response of the ITCZ
829 to Extratropical Thermal Forcing: Idealized Slab-Ocean Experiments with a GCM. *J.*
830 *Climate*, **21**, 3521–3532.

831 Kang, S.M., D.M.W. Frierson, and I.M. Held, 2009: The Tropical Response to
832 Extratropical Thermal Forcing in an Idealized GCM: The Importance of Radiative
833 Feedbacks and Convective Parameterization. *J. Atmos. Sci.*, **66**, 2812–2827.

834 Kang S.M., L.M. Polvani, J.C. Fyfe, and M. Sigmond, 2011: Impact of polar ozone
835 depletion on subtropical precipitation. *Science*, **332**, 951–954.

836 Kanner, L.C., S.J. Burns, H. Cheng, and R.L. Edwards, 2012: High-latitude forcing of the
837 South American summer monsoon during the last glacial. *Science*, **335**, 570-573.

838 Kanner, L.C., S.J. Burns, H. Cheng, R.L. Edwards and M. Vuille, 2013: High-resolution
839 variability of the South American summer monsoon over the last seven millennia:
840 Insights from a speleothem record from the central Peruvian Andes. *Quat. Sci., Rev.*,
841 **75**, 1-10.

842 Kaplan, J.O., P.W. Kubik, K.G. Ellis, W.F. Ruddiman, J. Lerner, and K.K. Goldewijk
843 2011: Holocene carbon emissions as a result of anthropogenic land cover change, *The*
844 *Holocene*, **21**, 775-791.

845 Karpechko, A. Yu., N.P. Gillett, M. Dall'Amico, and L.J. Gray, 2010: Southern
846 Hemisphere atmospheric circulation response to the El Chichón and Pinatubo
847 eruptions in coupled climate models. *Q.J.R. Meteorol. Soc.*, **136**, 1813–1822.

848 Kirchner, I., G.L. Stenchikov, H.-F. Graf, A. Robock, and J.C. Antuña, 1999: Climate
849 model simulation of winter warming and summer cooling following the 1991 Mount
850 Pinatubo volcanic eruption, *J. Geophys. Res.*, **104**, 19039–19055.

851 Krivova, N.A., L. Balmaceda, and S.K. Solanki, 2007: Reconstruction of solar total
852 irradiance since 1700 from the surface magnetic flux, *Astron. Astrophys.*, **467**, 335-
853 346.

854 Lacis, A., J. Hansen, and M. Sato, 1992: Climate forcing by stratospheric aerosols.
855 *Geophys. Res. Lett.*, **19**, 1607-1610.

856 Ledru, M.P., V. Jomelli, P. Samaniego, M. Vuille, S. Hidalgo, M. Herrera, and C. Ceron,
857 2013: The Medieval Climate Anomaly and the Little Ice Age in the eastern
858 Ecuadorian Andes. *Climate Past*, **9**, 4295.

859 Lucht, W., I.C. Prentice, R.B. Myneni, S. Sitch, P. Friedlingstein, W. Cramer, P.
860 Bousquet, W. Buermann, and B. Smith, 2002: Climatic control of the high-latitude
861 vegetation greening trend and Pinatubo effect. *Science*, **296**, 1687-1689.

862 Ludlow, F., A.R. Stine, P. Leahy, E. Murphy, P.A. Mayewski, D. Taylor, and G. Kiely,
863 2013: Medieval Irish chronicles reveal persistent volcanic forcing of severe winter
864 cold events, 431–1649 CE. *Environ. Res. Lett.*, **8**, 024035.

865 Man, W., T. Zhou, and J.H. Jungclaus, 2014: Effects of Large Volcanic Eruptions on
866 Global Summer Climate and East Asian Monsoon Changes during the Last
867 Millennium: Analysis of MPI-ESM Simulations. *J. Climate*, **27**, 7394–7409.

868 Mann, M.E., M.A. Cane, S.E. Zebiak, and A. Clement, 2005: Volcanic and Solar Forcing
869 of the Tropical Pacific Over the Past 1000 Years, *J. Climate*, **18**, 447-456.

870 Marengo J.A., B. Liebmann, V.E. Kousky, N.P. Filizola, and I.C. Wainer, 2001: Onset
871 and end of the rainy season in the Brazilian Amazon basin, *J. Climate*, **14**, 833–852.

872 Marengo, J. A., and Coauthors, 2012: Recent developments on the South American
873 monsoon system. *Int. J. Climatol.*, **32**, 1–21.

874 Miller, G.H., and Coauthors, 2012: Abrupt onset of the Little Ice Age triggered by
875 volcanism and sustained by sea-ice/ocean feedbacks, *Geophys. Res. Lett.*, **39**,
876 L02708.

877 Minnis, P., E.F. Harrison, L.L. Stowe, G.G. Gison, F.M. Denn, D.R. Doelling, and W.L.
878 Smith Jr., 1993: Radiative climate forcing by the Mount Pinatubo eruption, *Science*,
879 **259**, 1411-1415.

880 Neukom, R., and J. Gergis, 2012: Southern Hemisphere high-resolution palaeoclimate
881 records of the last 2000 years. *The Holocene*, **22**, 501-524.

882 Nogués -Paegle J, and K. Mo, 1997: Alternating wet and dry conditions over South
883 America during summer. *Mon. Wea. Rev.*, **125**, 279–291.

884 Nogués-Paegle, J., and Coauthors, 2002: Progress in Pan American CLIVAR research:
885 Understanding the South American monsoon. *Meteorologica*, **27**, 3-32.

886 Novello, V.F., F.W. Cruz, I. Karmann, S.J. Burns, N.M., Stríkis, M. Vuille, H. Cheng,
887 R.L. Edwards, R.V. Santos, E. Frigo, and E.A.S. Barreto, 2012: Multidecadal climate
888 variability in Brazil’s Nordeste during the last 3000 years based on speleothem
889 isotope records. *Geophys. Res. Lett.*, **39**, L23706.

890 Oman, L., A. Robock, G. Stenchikov, G.A. Schmidt, and R. Ruedy, 2005: Climatic
891 response to high-latitude volcanic eruptions. *J. Geophys. Res.*, **110**, D13103.

892 Oman, L., A. Robock, G.L. Stenchikov, and T. Thordarson, 2006: High-latitude
893 eruptions cast shadow over the African monsoon and the flow of the Nile. *Geophys.*
894 *Res. Lett.*, **33**, L18711.

895 Peng, Y., C. Shen, W.C. Wang, and Y. Xu, 2010: Response of Summer Precipitation over
896 Eastern China to Large Volcanic Eruptions. *J. Climate*, **23**, 818–824.

897 Pollack, J. B., O.B. Toon, C. Sagan, A. Summers, B. Baldwin, and W. Van Camp, 1976:
898 Volcanic explosions and climatic change: A theoretical assessment, *J. Geophys. Res.*,
899 **81**, 1071–1083.

900 Pollack, J. B., O.B. Toon, and D. Wiedman, 1981: Radiative properties of the background
901 stratospheric aerosols and implications for perturbed conditions, *Geophys. Res. Lett.*,
902 **8**, 26–28.

903 Pongratz, J., C. Reick, T. Raddatz, and M. Claussen, 2008: A global land cover
904 reconstruction AD 800 to 1992 – Technical description, *Rep. Earth Syst. Sci.*, **51**,
905 Max Planck Institute for Meteorology, Hamburg , Germany .

906 Robock, A., and J. Mao, 1992: Winter warming from large volcanic eruptions. *Geophys.*
907 *Res. Lett.*, **19**, 2405-2408.

908 Robock, A., and M.P. Free, 1995: Ice cores as an index of global volcanism from 1850
909 to the present, *J. Geophys. Res.*, **100**, 11549–11567.

910 Robock, A., and J. Mao, 1995: The volcanic signal in surface temperature observations.
911 *J. Climate*, **8**, 1086-1103.

912 Robock, A. 2000: Volcanic eruptions and climate, *Rev. Geophys.*, **38**, 191–219.

913 Robock, A., 2003: Volcanoes: Role in climate. in *Encyclopedia of Atmospheric Sciences*,
914 J. Holton, J. A. Curry, and J. Pyle, Eds., (Academic Press, London).

915 Robock, A., T. Adams, M. Moore, L. Oman, and G. Stenchikov, 2007: Southern
916 Hemisphere atmospheric circulation effects of the 1991 Mount Pinatubo eruption,
917 *Geophys. Res. Lett.*, **34**, L23710.

918 Russell, G.L., J.R. Miller, and D.H. Rind, 1995: A coupled atmosphere-ocean model for
919 transient climate change, *Atmosphere-ocean*, **33**, 683-730.

920 Sato, M., J.E. Hansen, M.P. McCormick, and J.B. Pollack 1993: Stratospheric aerosol
921 optical depth, 1850-1990. *J. Geophys. Res.* **98**, 22987-22994.

922 Savarino, J., A. Romero, J. Cole-Dai, S. Bekki, and M. H. Thiemens 2003: UV induced
923 mass-independent sulfur isotope fractionation in stratospheric volcanic sulfate.
924 *Geophys. Res. Lett.*, **30**, 2131.

925 Schmidt, G.A., A.N. LeGrande, and G. Hoffmann, 2007: Water isotope expressions of
926 intrinsic and forced variability in a coupled ocean-atmosphere model. *J. Geophys.*
927 *Res.*, **112**, D10103.

928 Schmidt, G.A., and Coauthors, 2011: Climate forcing reconstructions for use in PMIP
929 simulations of the last millennium (v1.0). *Geosci. Model Dev.*, **4**, 33-45.

930 Schmidt, G.A., and Coauthors, 2012: Climate forcing reconstructions for use in PMIP
931 simulations of the Last Millennium (v1.1). *Geosci. Model Dev.*, **5**, 185-191.

932 Schmidt, G.A., and Coauthors, 2014a: Configuration and assessment of the GISS
933 ModelE2 contributions to the CMIP5 archive. *J. Adv. Model. Earth Syst.*, **6**.

934 Schmidt, G.A., and Coauthors, 2014b: Using paleo-climate comparisons to constrain
935 future projections in CMIP5. *Climate Past*, **10**, 221-250.

936 Schneider U., A. Becker, P. Finger, A. Meyer-Christoffer, M. Ziese, and B. Rudolf, 2013:
937 GPCP's new land surface precipitation climatology based on quality-controlled in
938 situ data and its role in quantifying the global water cycle. *Theor. App. Climatol.*, **115**,
939 15-40.

940 Schurer, A.P., S.F.B. Tett, and G.C. Hegerl, 2014: Small influence of solar variability on
941 climate over the past millennium. *Nature Geosci.*, **7**, 104-108.

942 Seth, A., M. Rojas, and S. A. Rauscher, 2010: CMIP3 projected changes in the annual
943 cycle of the South American monsoon. *Climatic Change*, **98**, 331–357.

944 Shindell, D.T., G.A. Schmidt, M.E. Mann, and G. Faluvegi, 2004: Dynamic winter
945 climate response to large tropical volcanic eruptions since 1600. *J. Geophys. Res.*,
946 **109**, D05104.

947 Silva A.E., and L.M.V. Carvalho, 2007: Large-scale index for South America Monsoon
948 (LISAM), *Atmos. Sci. Lett.*, **8**, 51–57.

949 Steinhilber, F., J. Beer, and C. Fröhlich, 2009: Total solar irradiance during the Holocene,
950 *Geophys. Res. Lett.*, **36**, L19704.

951 Stenchikov, G.L., I. Kirchner, A. Robock, H.-F. Graf, J.C. Antuña, R.G. Grainger, A.
952 Lambert, and L. Thomason, 1998: Radiative forcing from the 1991 Mount Pinatubo
953 volcanic eruption. *J. Geophys. Res.*, **103**, 13837–13857.

954 Stenchikov, G., K. Hamilton, A. Robock, V. Ramaswamy, and M. D. Schwarzkopf,
955 2004: Arctic Oscillation response to the 1991 Pinatubo eruption in the SKYHI GCM
956 with a realistic quasi-biennial oscillation, *J. Geophys. Res.*, **109**, D03112.

957 Stenchikov, G., K. Hamilton, R. J. Stouffer, A. Robock, V. Ramaswamy, B. Santer, and
958 H.F. Graf, 2006: Arctic Oscillation response to volcanic eruptions in the IPCC AR4
959 climate models, *J. Geophys. Res.*, **111**, D07107.

960 Stothers, R.B., and M.R. Rampino, 1983: Historic volcanism, European dry fogs, and
961 Greenland acid precipitation, 1500 B.C. to A.D. 1500. *Science*, **222**, 411-413.

962 Thompson, L.G., E. Mosley-Thompson, M.E. Davis, P.-N. Lin, K.A. Henderson, J. Cole-
963 Dai, J.F. Bolzan, and K.-b. Liu, 1995: Late glacial stage and Holocene tropical ice
964 core records from Huascarán, Peru. *Science*, **269**, 46-50.

965 Thompson, L.G., and Coauthors, 1998: A 25,000-year tropical climate history from
966 Bolivian ice cores. *Science*, **282**, 1858-1864.

967 Thompson, L.G., E. Mosley-Thompson, H. Brecher, M. Davis, B. Leon, D. Les, P.N. Lin,
968 T. Mashiotta, and K. Mountain, 2006: Abrupt tropical climate change: Past and
969 present. *Proc. Nat. Acad. Sci.*, **103**, 10536-10543.

970 Timmreck, C, 2012: Modeling the climatic effects of large explosive volcanic eruptions,
971 *Wiley Interdiscip. Rev. Climate Change*, **3**, 545–564.

972 Trenberth, K. E., and A. Dai, 2007: Effects of Mount Pinatubo volcanic eruption on the
973 hydrological cycle as an analog of geoengineering. *Geophys. Res. Lett.*, **34**, L15702.

974 Turco, R.P., R.C. Whitten, and O.B. Toon, 1982: Stratospheric aerosols: Observation and
975 theory. *Rev. Geophys.*, **20**, 233–279.

976 Van Breukelen, M.R., H.B. Vonhof, J.C. Hellstrom, W.C.G. Wester, and D. Kroon, 2008:
977 Fossil dripwater in stalagmites reveals Holocene temperature and rainfall variation in
978 Amazonia. *Earth Planet. Sci. Lett.*, **275**, 54-60.

979 Vera C.S., and Coauthors, 2006: Toward a Unified View of the American Monsoon
980 Systems. *J. Climate*, **19**, 4977–5000.

981 Vimeux, F., R. Gallaire, S. Bony, G. Hoffmann, and J.C.H. Chiang, 2005: What are the
982 climate controls on δD in precipitation in the Zongo Valley (Bolivia)? Implications
983 for the Illimani ice core interpretation, *Earth Planet. Sci. Lett.*, **240**, 205–220.

984 Vimeux F., P. Ginot, M. Schwikowski, M. Vuille, G. Hoffmann, L.G. Thompson, U.
985 Schotterer, 2009: Climate variability during the last 1000 years inferred from Andean
986 ice cores: A review of methodology and recent results. *Palaeogeogr. Palaeoclimatol.*
987 *Palaeoecol.*, **281**, 229–241.

988 Vuille, M., R.S. Bradley, M. Werner, R. Healy, and F. Keimig, 2003: Modeling $d^{18}O$ in
989 precipitation over the tropical Americas: 1. Interannual variability and climatic
990 controls. *J. Geophys. Res.*, **108**, 4174.

991 Vuille, M., and M. Werner, 2005: Stable isotopes in precipitation recording South
992 American summer monsoon and ENSO variability– observations and model results,

993 *Climate Dynam.*, **25**, 401–413.

994 Vuille, M., S.J. Burns, B.L. Taylor, F.W. Cruz, B.W. Bird, M.B. Abbott, L.C. Kanner, H.
995 Cheng, and V.F. Novello, 2012: A review of the South American monsoon history as
996 recorded in stable isotopic proxies over the past two millennia. *Climate Past*, **8**, 1309-
997 1321.

998 Wilmes, S.B., C.C. Raible, and T.F. Stocker, 2012: Climate variability of the mid- and
999 high-latitudes of the Southern Hemisphere in ensemble simulations from 1500 to
1000 2000 AD. *Climate Past*, **8**, 373-390.

1001 Yoshimori, M., T. F. Stocker, C. Raible, and M. Renold, 2005: Externally forced and
1002 internal variability in ensemble climate simulations of the Maunder Minimum, *J.*
1003 *Climate*, **18**, 4253– 4270.

1004 Zhang D., R. Blender, and K. Fraedrich, 2012: Volcanoes and ENSO in millennium
1005 simulations: global impacts and regional reconstructions in East Asia. *Theor. Appl.*
1006 *Climatol.*, **111**, 437-454.

1007 Zhou, J., and K.-M. Lau, 1998: Does a monsoon climate exist over South America? *J.*
1008 *Climate*, **11**, 1020-1040.

1009 Zielinski, G.A., 1995: Stratospheric loading and optical depth estimates of explosive
1010 volcanism over the last 2100 years derived from the Greenland Ice Sheet Project 2 ice
1011 core, *J. Geophys. Res.*, **100**, 20937–20955.

1012 Zielinski, G.A., 2000: Use of paleo-records in determining variability within the
1013 volcanism-climate system. *Quat. Sci. Rev.*, **19**, 417–438.

1014

1015

1016 Table 1: Time of Eruptions and Global Aerosol Optical Depth (AOD) from Crowley and
 1017 Unterman (2013).

1018



1019

Table 1. List of LM Eruptions

Start Date of Eruption ^a	Seasons in LM Composite		max AOD ^b
	DJF ^c	JJA	
Jan 971	972	971-972	0.219
Jan 1193	1194	1193-1194	0.183
Jul 1228	1229-1231	1229-1230	0.376
Oct 1257	1258-1260	1258-1259	0.691
Jan 1286	1287-1288	1286-1287	0.283
Jul 1455	1456-1458	1456-1458	0.444
Jan 1600	1601	1600	0.169
Jan 1641	1642	1641-1642	0.229
May 1673	1674	1674	0.213
Apr 1694	1695-1697	1694-1696	0.24
Jan 1809	1810-1811	1809-1810	0.301
May 1815	1816-1818	1815-1817	0.465
May 1835	1836	1835-1836	0.232
Jan 1883	1884	1884	0.196
Jul 1963	1964	1964	0.114
Jun 1991	1992	1992	0.177

^a. Start of Eruptions dates are based on when they can be first identified in the Crowley time-series averaged over the latitude band from 30 ° S to 20 ° N.

^b. Maximum AOD over the same latitude band in ModelE2-R for the duration of the forcing.

^c. December in year prior to listed date.

1020

1021

1022

1023

1024

1025

1026

1027

1028

1029 **List of Figure Captions**

1030

1031 **Figure. 1.** Aerosol Optical Depth (AOD) used to force the NASA GISS ModelE2-R over
1032 the Last Millennium and focused on 1050-1999 (Crowley+Sato) as discussed in text.
1033 AOD is the vertically integrated (15-35 km) and latitudinal average from 30°S to 20°N.
1034 Note difference in vertical scale between graphs. Orange dashed line marks the AOD
1035 threshold for defining a LM eruption in the present study. Eruption events defined in text
1036 must sustain the threshold AOD for at least one year, so not all events above the orange
1037 dashed line are used in the composites.

1038

1039

1040 **Figure. 2.** Cartoon sketch of the South American climate system. SAMS box is drawn
1041 over the domain from 75° to 45° W, 20° S to 0° and used for Figure 9 and 12. Filled
1042 color indicates the ratio of precipitation that falls during the selected season to the entire
1043 year (December-November). Values for the precipitation ratio, and for the wind field
1044 (m/s), are averages from 48 selected 30-year climatologies during the Last Millennium
1045 simulations that surround volcanic eruption events (16 eruptions within three ensemble
1046 members) that are used for the Last Millennium composites.

1047

1048 **Figure. 3.** Composite tropical (25°S to 25°N) response in (a) Temperature and (b)
1049 Precipitation using El Chichón and Mt. Pinatubo. Fill color denotes monthly observed
1050 anomalies using (a) GISTEMP and (b) GPCP products with 18-month running average in
1051 observations (solid black), ModelE2-R ensemble mean (solid orange), and six individual

1052 ensemble members (dashed grey). Anomalies base-lined to give a mean of zero over
1053 displayed period.

1054

1055 **Figure. 4.** Temperature change (°C) for each L20 eruption (labeled on plot) for JJA in
1056 GISTEMP (first column), model (second column), and during DJF for GISTEMP (third
1057 column) and model (fourth column). All plots use ENSO-removal procedure described in
1058 text and the model results are shown for six-member ensemble mean.

1059

1060 **Figure. 5.** As in Figure 4, except for Precipitation change (mm/day).

1061

1062 **Figure. 6.** Seasonal cycle (DJF minus JJA) of $\delta^{18}\text{O}_p$ in **a)** GNIP and **b)** ModelE2-R
1063 (colored). Precipitation is contoured in solid at 6 mm/day and dashed at -6mm/day. GNIP
1064 data selected with a minimum of 70 reported $\delta^{18}\text{O}_p$ values at a given station from 1960-
1065 present. Model precipitation and $\delta^{18}\text{O}_p$ climatology from 1960-2005 and GPCP
1066 precipitation over the same period (1979-2005 over ocean).

1067

1068 **Figure. 7.** Last Millennium post-volcanic temperature composite (°C) averaged over all
1069 48 events during **a)** DJF and **b)** JJA from GISS ModelE2-R using procedure described in
1070 text.

1071

1072 **Figure. 8.** Last Millennium post-volcanic precipitation composite (mm/day) with all
1073 eruption events during **a)** DJF and **b)** JJA from GISS ModelE2-R using procedure
1074 described in text.

1075

1076 **Figure. 9. a)** Average Temperature during DJF within the SAMS region (red, 75° to
1077 45°W, 20°S to 0°N) and equatorial South America during JJA (blue, 75° to 45°W, 0 to
1078 12°N) plotted against the peak AOD for all 16 eruptions (each point averaged over three
1079 ensemble members with the three member spread shown as horizontal bars) and **b)** For
1080 precipitation.

1081

1082 **Figure. 10.** Last Millennium post-volcanic oxygen isotope in precipitation ($\delta^{18}\text{O}_p$)
1083 composite (per mil) with all eruption events during **a)** DJF and **b)** JJA from GISS
1084 ModelE2-R using procedure described in text.

1085

1086 **Figure. 11.** Last Millennium Hovmöller diagram (10 years, time moving forward going
1087 upward, with year number labeled next to each month) for **a)** temperature anomaly (°C)
1088 **b)** precipitation anomaly (mm/day) using procedure described in text. Solid black lines
1089 mark closest January to start of each eruption used in composite. **c)** Same as panel b,
1090 except zoomed in on 10 °S to 10 °N and over 3 years of time beginning with the January
1091 closest to each eruption. Red line in panel c shows latitude of maximum climatological
1092 precipitation as a function of time of year. All results zonally averaged in model from
1093 76.25° to 46.75° W. **d)** Last Millennium Hovmöller diagrams for oxygen isotopes in
1094 precipitation (per mil).

1095

1096 **Figure. 12.** Frequency distribution of 100 random 48-event composites in LM control
1097 simulation of ModelE2-R (blue) for temperature (top row), precipitation (middle), and

1098 oxygen isotopes in precipitation (bottom) for DJF (left column) and JJA (right column).
1099 Results averaged over same domains as in Figure 9. Normal distribution with a mean and
1100 standard deviation equal to that of the data shown in dark green. Red line shows the
1101 single 48-event composite used in this study, with the distribution of 16 volcanic
1102 eruptions (each averaged over three ensemble members) in grey.

1103

1104 **Figure. 13.** Post-volcanic LM composite of Sea Level Pressure (SLP, hPa) anomaly for
1105 **a) DJF b) JJA** (vector magnitude below plot, m/s).

1106

1107 **Figure. 14.** Last Millennium post-volcanic composite of land evaporation (mm/day) for
1108 **a) DJF b) JJA**, and the energy of river discharge (in 10^{11} Watts) for **c) DJF d) JJA**. For
1109 flux conversion, note that the area of each grid cell in ModelE2-R at latitude ϕ is
1110 approximately $(6.2 \times 10^{10} \text{ m}^2) \cos \phi$.

1111

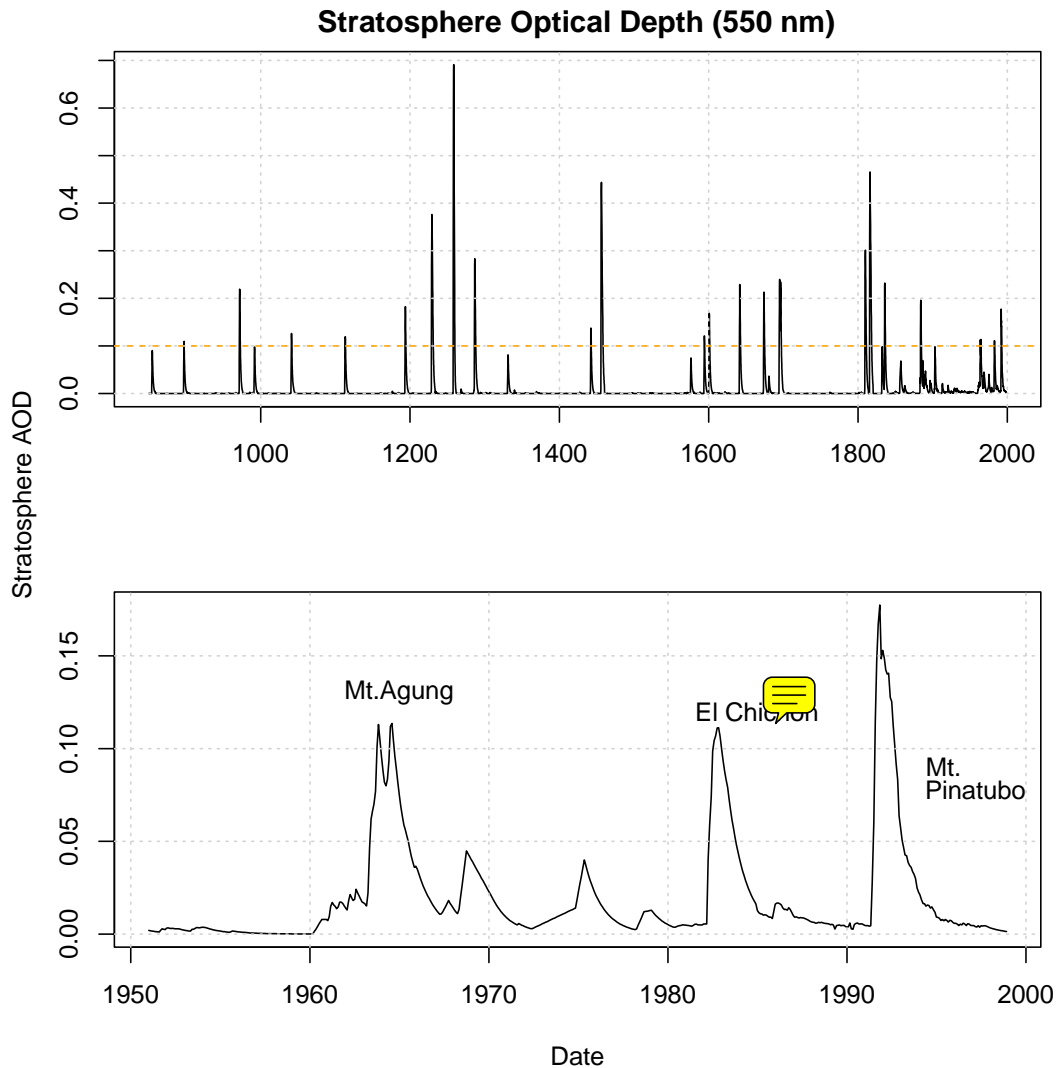
1112

1113

1114

1115

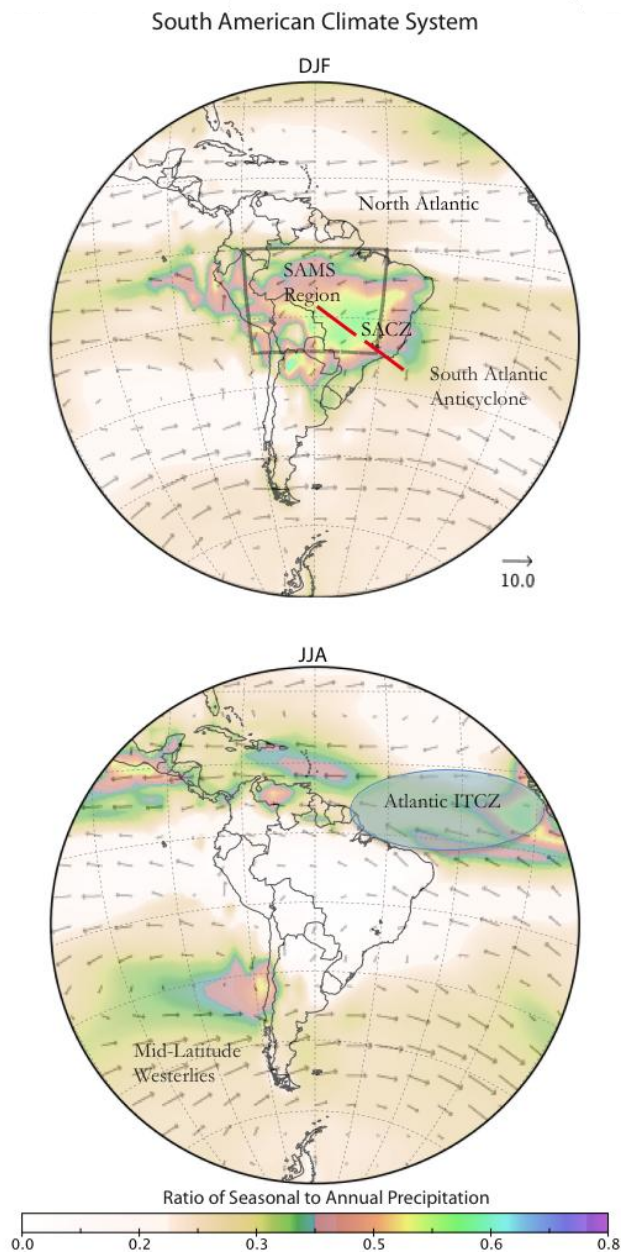
1116



1117

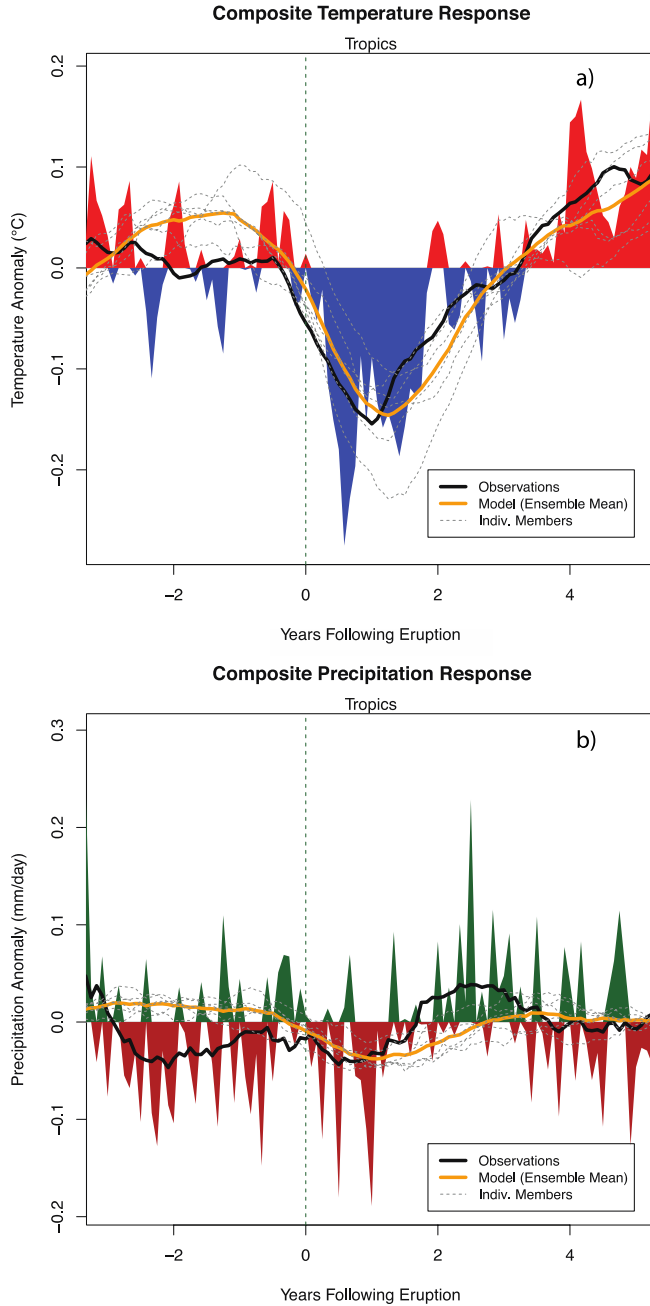
1118

1119 **Figure. 1.** Aerosol Optical Depth (AOD) used to force the NASA GISS ModelE2-R over
 1120 the **Last Millennium** and focused on 1050-1999 (Crowley+Sato) as discussed in text.
 1121 AOD is the vertically integrated (15-35 km) and latitudinal average from 30°S to 20°N.
 1122 Note difference in vertical scale between graphs. Orange dashed line marks the AOD
 1123 threshold for defining a LM eruption in the present study. Eruption events defined in text
 1124 must **sustain the threshold AOD for at least one year**, so not all events above the orange
 1125 dashed line are used in the composites.



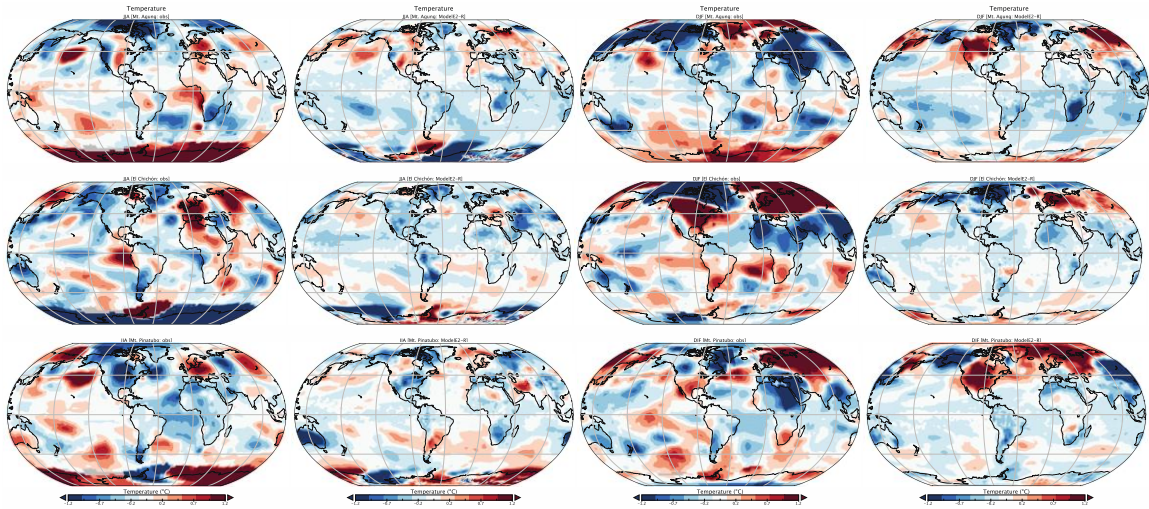
1126

1127 **Figure. 2.** Cartoon sketch of the South American climate system. **SAMS** box is drawn
 1128 over the domain from 75° to 45° W, 20° S to 0° and used for Figure 9 and 12. Filled
 1129 color indicates the ratio of precipitation that falls during the selected season to the entire
 1130 year (December-November). Values for the precipitation ratio, and for the wind field
 1131 (m/s), are averages from 48 selected 30-year climatologies during the Last Millennium
 1132 simulations that surround volcanic eruption events (16 eruptions within three ensemble
 1133 members) that are used for the Last Millennium composites.
 1134



1136

1137 **Figure 3.** Composite tropical (25°S to 25°N) response in (a) Temperature and (b)
 1138 Precipitation using El Chichón and Mt. Pinatubo. Fill color denotes monthly observed
 1139 anomalies using (a) GISTEMP and (b) GPCP products, with 18-month running average
 1140 in observations (solid black), ModelE2-R ensemble mean (solid orange), and six
 1141 individual ensemble members (dashed grey). Anomalies base-lined to give a mean of
 1142 zero over displayed period.



1143

1144 **Figure. 4.** Temperature change (°C) for each **L20** eruption (labeled on plot) for JJA in
 1145 GISTEMP (first column), model (second column), and during DJF for GISTEMP (third
 1146 column) and model (fourth column). All plots use ENSO-removal procedure described in
 1147 text and the model results are shown for six-member ensemble mean.
 1148

1149

1150

1151

1152

1153

1154

1155

1156

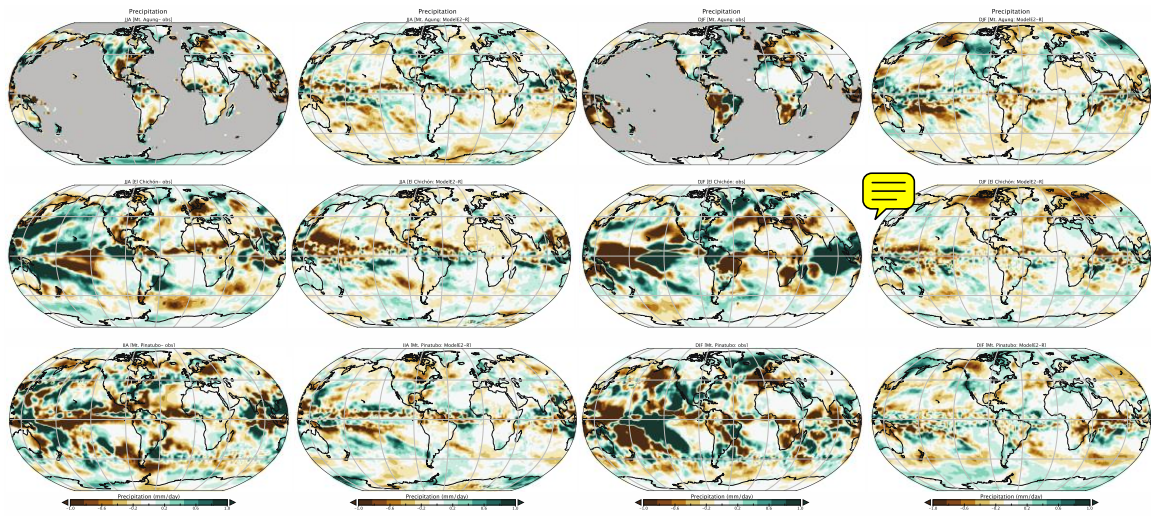
1157

1158

1159

1160

1161



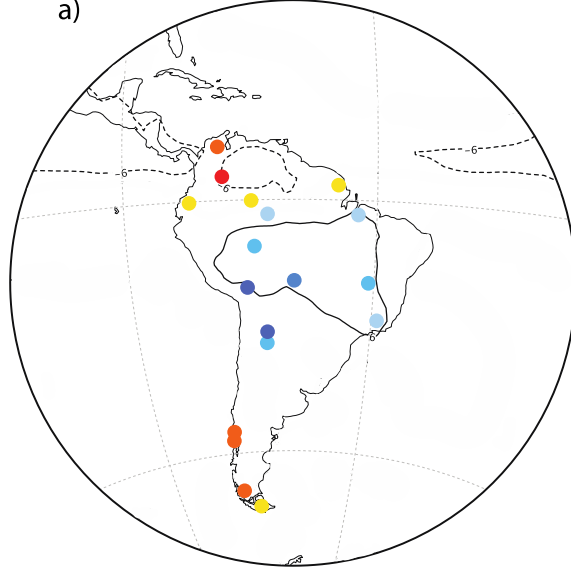
1162

1163 **Figure. 5.** As in Figure 4, except for Precipitation change (mm/day).

1164

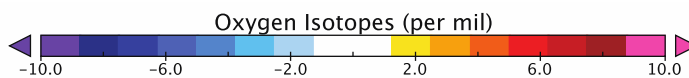
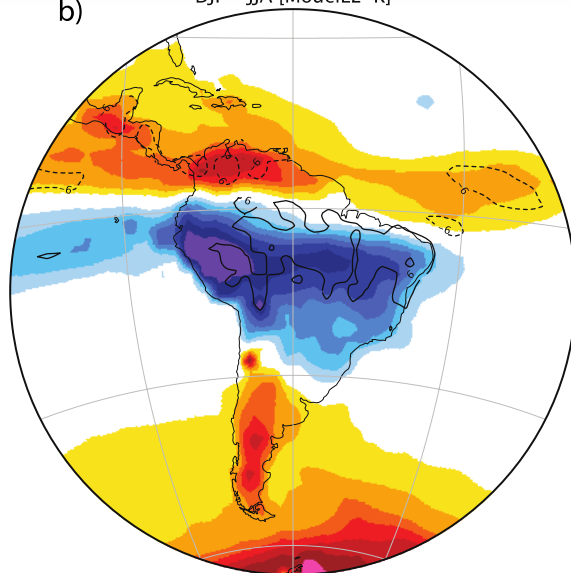
Oxygen Isotopes in Precipitation
DJF - JJA [GNIP]

a)



DJF - JJA [ModelE2-R]

b)



1165

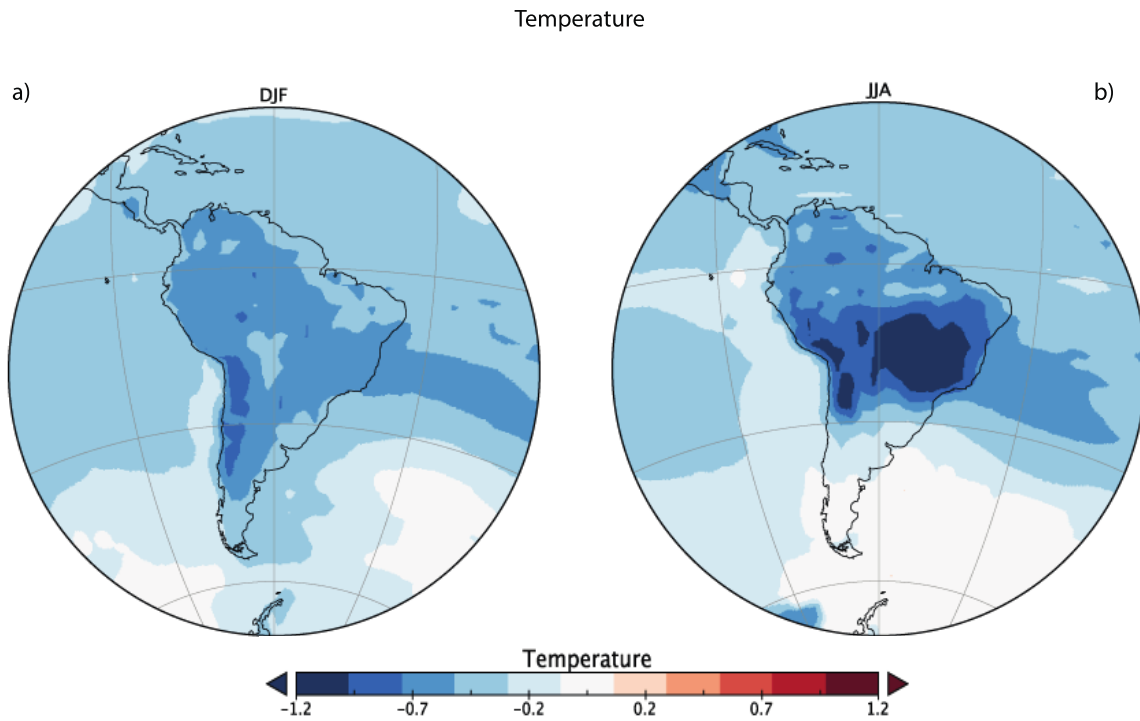
1166 **Figure. 6.** Seasonal cycle (DJF minus JJA) of $\delta^{18}\text{O}_p$ in **a) GNIP** and **b) ModelE2-R**
1167 (colored). Precipitation is contoured in solid at 6 mm/day and dashed at -6mm/day. GNIP
1168 data selected with a minimum of 70 reported $\delta^{18}\text{O}_p$ values at a given station from 1960-
1169 present. Model precipitation and $\delta^{18}\text{O}_p$ climatology from 1960-2005 and GPCP
1170 precipitation over the same period (1979-2005 over ocean).
1171

1172

1173

1174

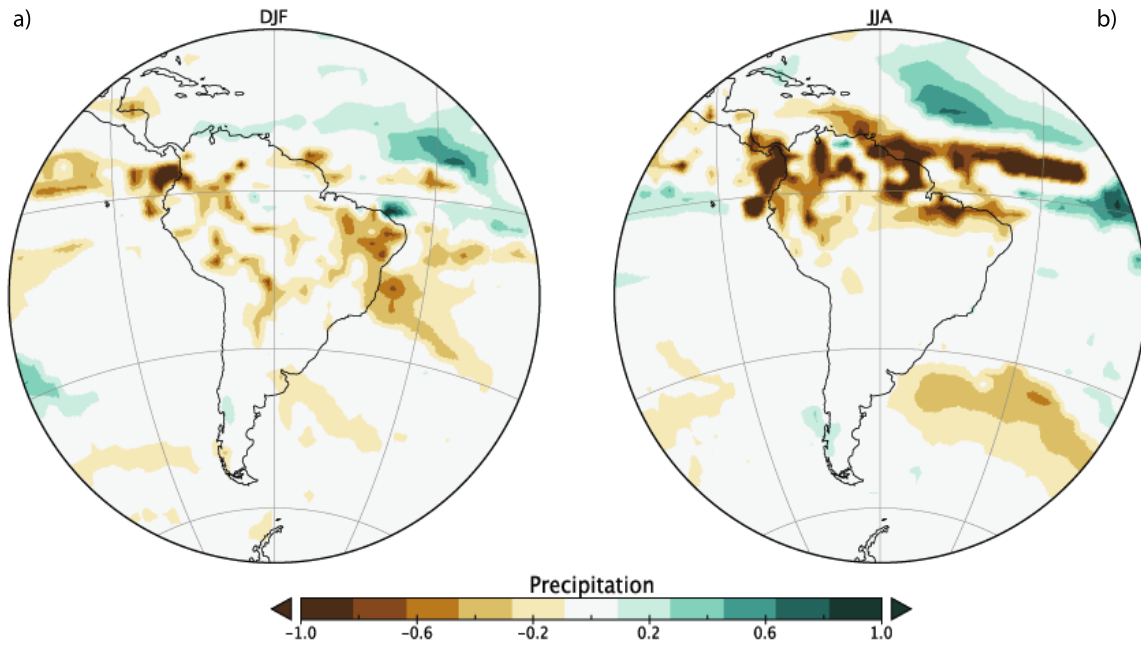
1175



1176

1177 **Figure. 7.** Last Millennium post-volcanic temperature composite ($^{\circ}\text{C}$) averaged over all
1178 48 events during **a) DJF** and **b) JJA** from GISS ModelE2-R using procedure described in
1179 text.
1180

Precipitation



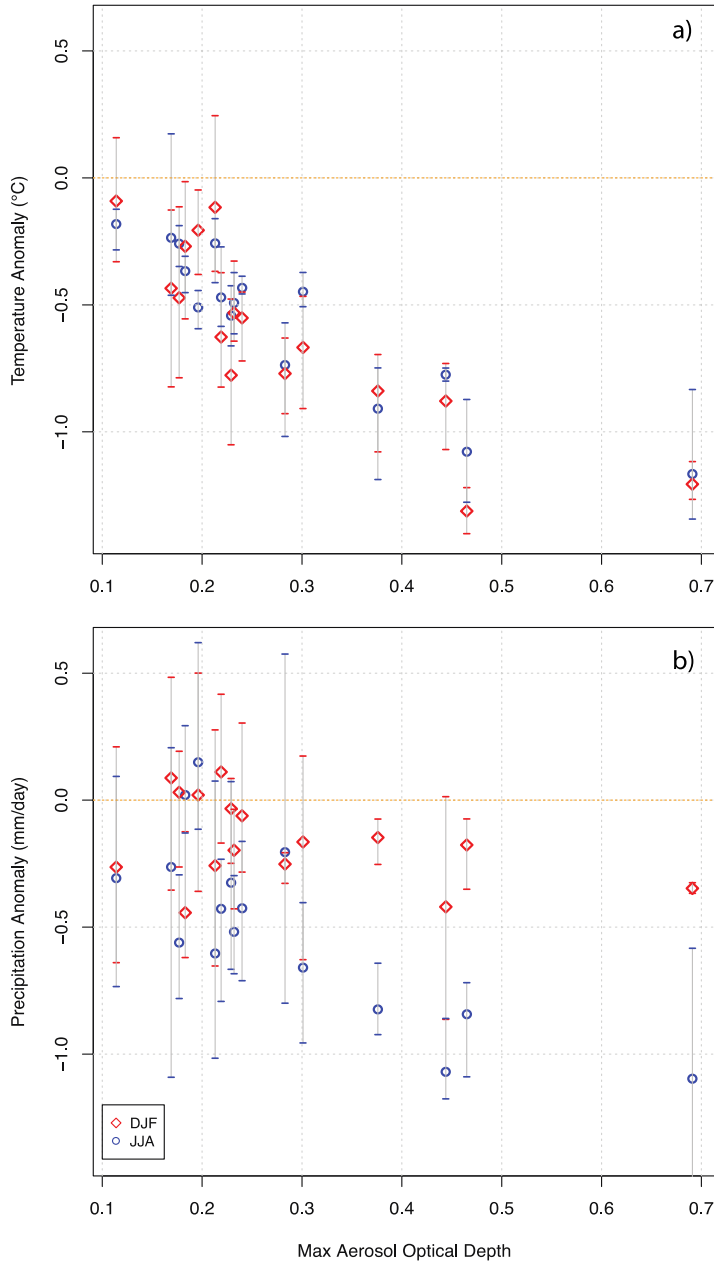
1181

1182 **Figure. 8.** Last Millennium post-volcanic precipitation composite (mm/day) with all
1183 eruption events during **a)** DJF and **b)** JJA from GISS ModelE2-R using procedure
1184 described in text.

1185

1186

1187

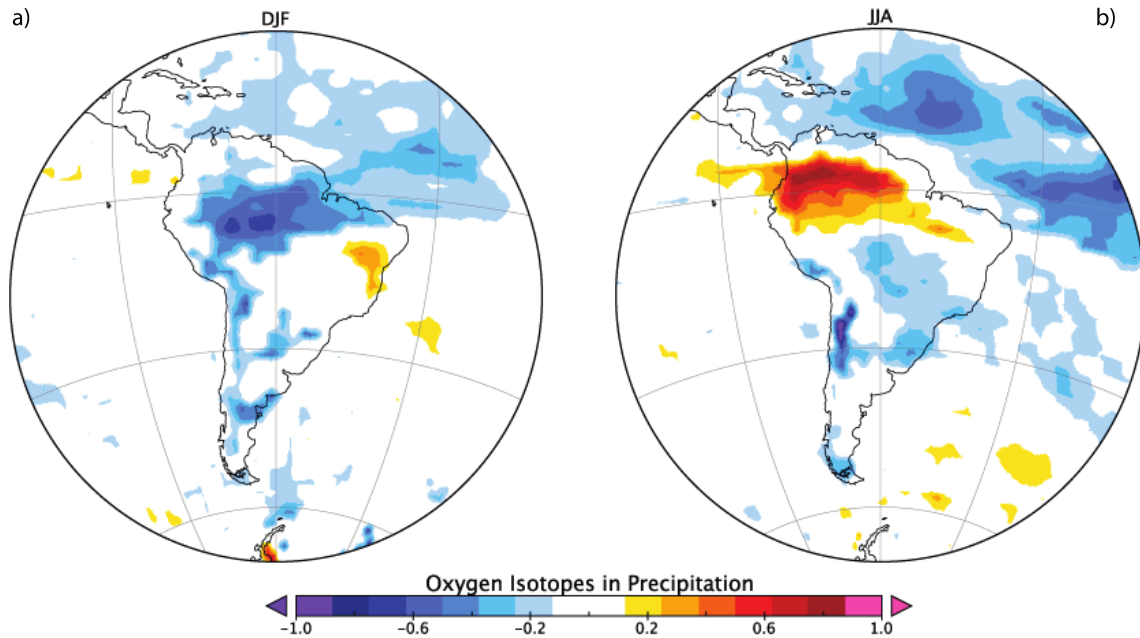


1188

1189 **Figure. 9. a)** Average Temperature during DJF within the SAMS region (red, 75° to
 1190 45°W, 20°S to 0°N) and equatorial South America during JJA (blue, 75° to 45°W, 0 to
 1191 12°N) plotted against the peak AOD for all 16 eruptions (each point averaged over three
 1192 ensemble members with the three member spread shown as horizontal bars) and **b)** For
 1193 precipitation.

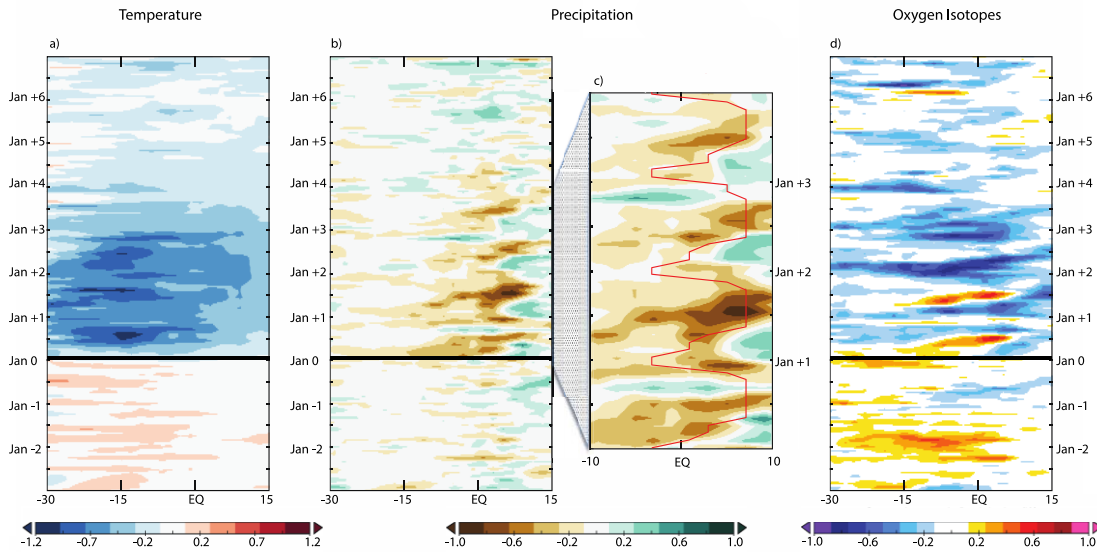
1194
1195
1196
1197
1198
1199
1200
1201

Oxygen Isotopes in Precipitation



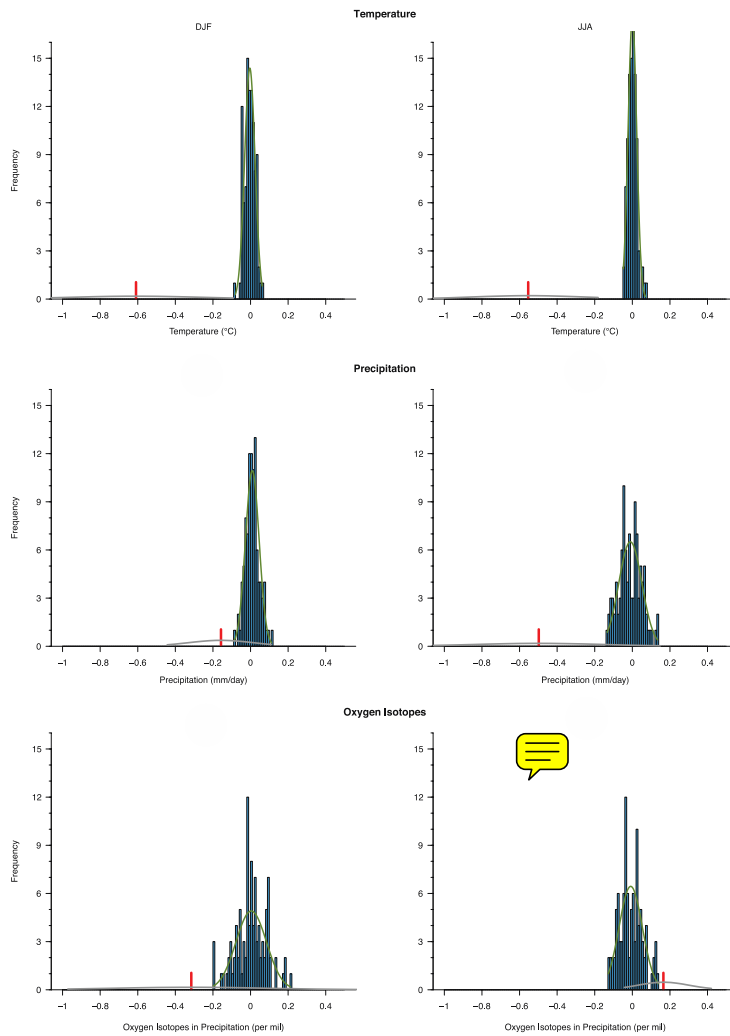
1202

1203 **Figure. 10.** Last Millennium **post-volcanic oxygen isotope** in precipitation ($\delta^{18}\text{O}_p$)
1204 composite (per mil) with all eruption events during **a)** DJF and **b)** JJA from GISS
1205 ModelE2-R using procedure described in text.
1206



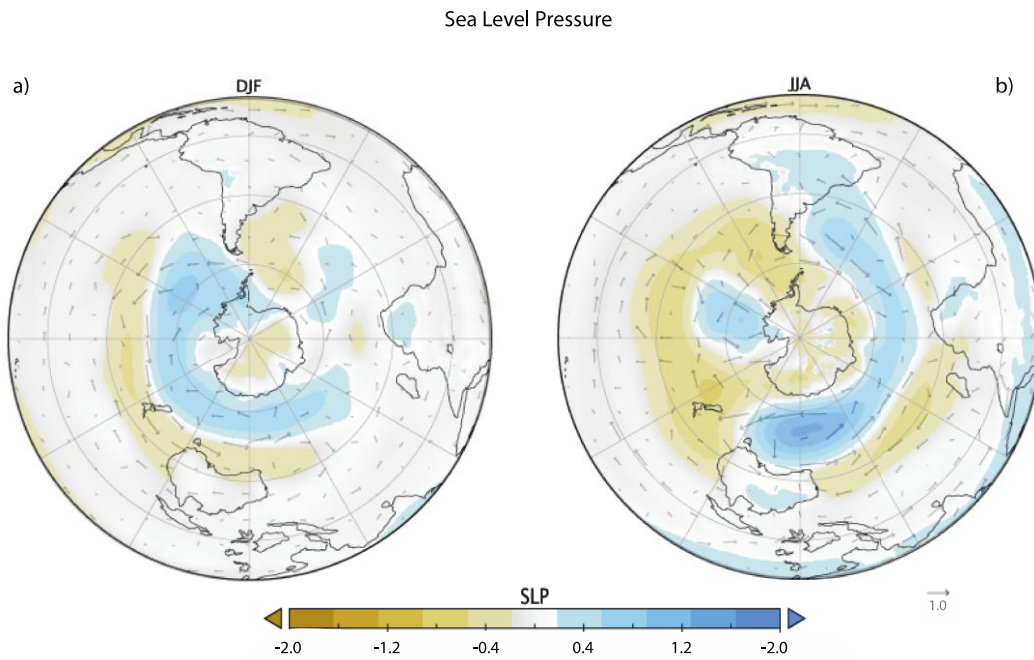
1207
 1208
 1209
 1210
 1211
 1212
 1213
 1214
 1215
 1216
 1217

Figure. 11. Last Millennium Hovmöller diagram (10 years, time moving forward going upward, with year number labeled next to each month) for **a)** temperature anomaly ($^{\circ}\text{C}$) **b)** precipitation anomaly (mm/day) using procedure described in text. Solid black lines mark closest January to start of each eruption used in composite. **c)** Same as panel b, except zoomed in on 10°S to 10°N and over 3 years of time beginning with the January closest to each eruption. Red line in panel c shows latitude of maximum climatological precipitation as a function of time of year. All results zonally averaged in model from 76.25° to 46.75°W . **d)** Last Millennium Hovmöller diagrams for oxygen isotopes in precipitation (per mil).



1218
 1219 **Figure. 12.** Frequency distribution of 100 random 48-event composites in LM control
 1220 simulation of ModelE2-R (blue) for temperature (top row), precipitation (middle), and
 1221 oxygen isotopes in precipitation (bottom) for DJF (left column) and JJA (right column).
 1222 Results averaged over same domains as in Figure 9. Normal distribution with a mean and
 1223 standard deviation equal to that of the data shown in dark green. Red line shows the
 1224 single 48-event composite used in this study, with the distribution of 16 volcanic
 1225 eruptions (each averaged over three ensemble members) in grey.

1226



1227

1228 **Figure. 13.** Post-volcanic LM composite of **Sea Level Pressure (SLP, hPa)** anomaly for
1229 **a) DJF b) JJA** (**vector magnitude below plot, m/s**).

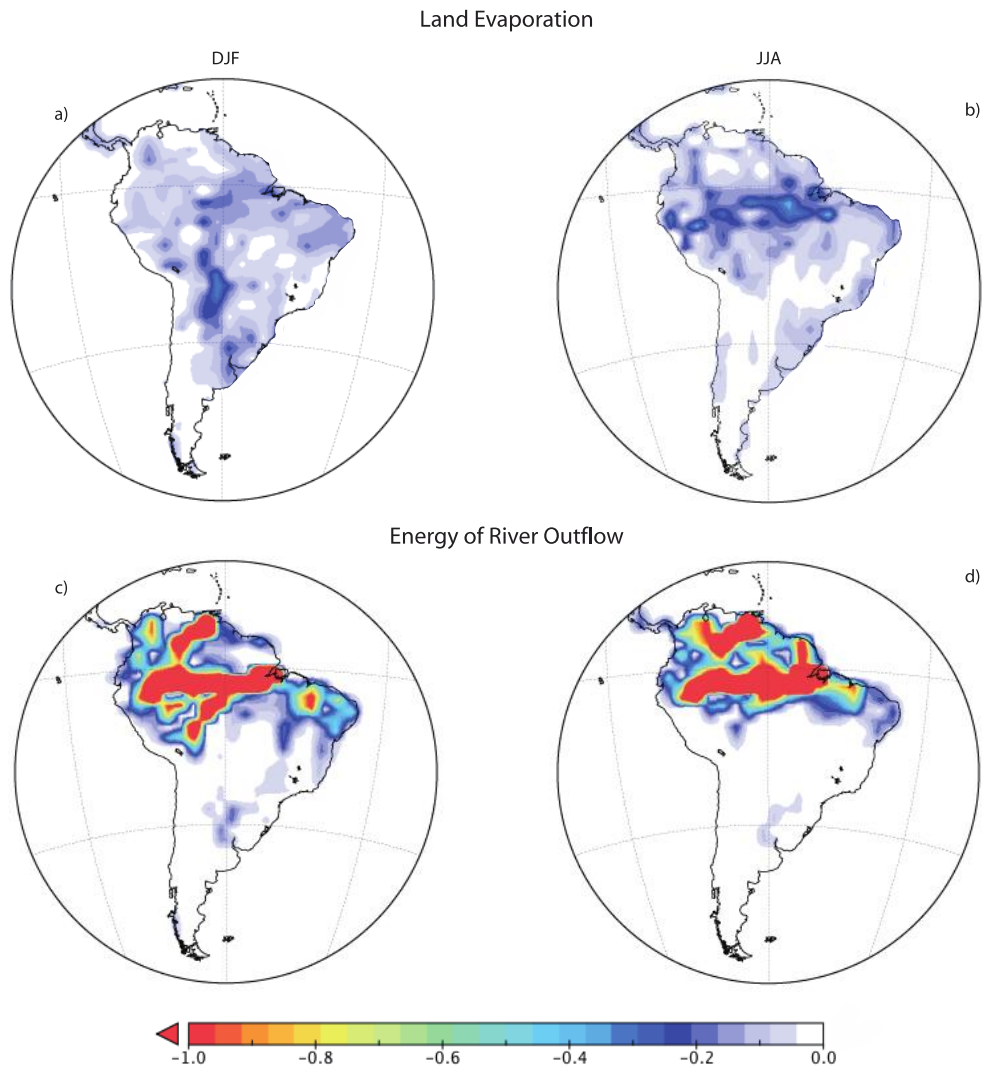
1230

1231

1232

1233

1234



1235

1236

1237 **Figure. 14.** Last Millennium post-volcanic composite of land evaporation (mm/day) for
1238 a) DJF b) JJA, and the energy of river discharge (in 10^{11} Watts) for c) DJF d) JJA. For
1239 flux conversion, note that the area of each grid cell in ModelE2-R at latitude ϕ is
1240 approximately $(6.2 \times 10^{10} \text{ m}^2) \cos \phi$.
1241

1242

1243

1244

Supplemental Material

[Click here to download Supplemental Material: JC_submit_ccolose_supp2.docx](#)